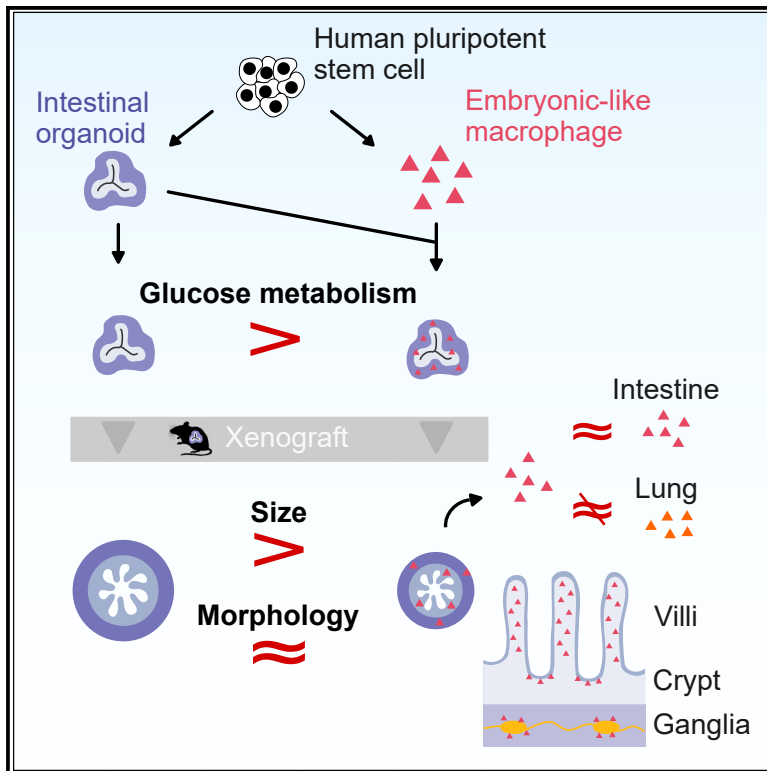


Developmental role of macrophages modeled in human pluripotent stem cell-derived intestinal tissue

Graphical abstract



Authors

Andrew T. Song, Renata H.M. Sindeaux, Yuanyi Li, ..., Elie Haddad, Luis Barreiro, Gregor Andelfinger

Correspondence

andthsong@hotmail.com (A.T.S.), gregor.andelfinger.med@ssss.gouv.qc.ca (G.A.)

In brief

Song et al. grew pluripotent stem cell-derived miniature intestinal tissue populated with macrophages. Macrophages within the tissue recapitulate aspects of microanatomical localization and transcriptomic changes observable in developing intestinal macrophages. They downregulate glycolysis of mesenchymal cells within the tissue. They also limit its growth without affecting the architecture.

Highlights

- PSC-derived multi-cell-type intestinal organoid populated with macrophages
- Recapitulate aspects of microanatomical localization and transcriptomic changes
- Macrophages in the organoid downregulate glycolysis of mesenchymal cells
- Macrophages in the organoid limit tissue growth without affecting the architecture



Article

Developmental role of macrophages modeled in human pluripotent stem cell-derived intestinal tissue

Andrew T. Song,^{1,2,*} Renata H.M. Sindeaux,^{1,6} Yuanyi Li,¹ Hicham Affia,¹ Tapan Agnihotri,^{1,5} Severine Leclerc,¹ Patrick Piet van Vliet,¹ Mathieu Colas,¹ Jean-Victor Guimond,⁷ Natalie Patey,⁸ Lara Feulner,¹ Jean-Sebastien Joyal,^{1,4,5} Elie Haddad,^{1,4} Luis Barreiro,^{1,3} and Gregor Andelfinger^{1,2,4,9,*}

¹Centre de Recherche, CHU Sainte-Justine, Montréal, QC, Canada

²Department of Anatomy and Cell Biology, McGill University, Montréal, QC, Canada

³Genetics Genomics and Systems Biology, University of Chicago, Chicago, IL, USA

⁴Département de Pédiatrie, Université de Montréal, Montréal, QC, Canada

⁵Department of Pharmacology and Therapeutics, McGill University, Montréal, QC, Canada

⁶Meakins Christie Laboratories, Department of Medicine, Department of Microbiology and Immunology, Department of Pathology Research Institute of McGill University Health Centre, Montréal, QC, Canada

⁷CLSC des Faubourgs, CIUSSS du Centre-Sud-de-l'Île-de-Montréal, Montréal, QC, Canada

⁸Department of Pathology, CHU Sainte-Justine, Université de Montréal, Montréal, QC, Canada

⁹Lead contact

*Correspondence: andthsong@hotmail.com (A.T.S.), gregor.andelfinger.med@ssss.gouv.qc.ca (G.A.)

<https://doi.org/10.1016/j.celrep.2023.113616>

SUMMARY

Macrophages populate the embryo early in gestation, but their role in development is not well defined. In particular, specification and function of macrophages in intestinal development remain little explored. To study this event in the human developmental context, we derived and combined human intestinal organoid and macrophages from pluripotent stem cells. Macrophages migrate into the organoid, proliferate, and occupy the emerging microanatomical niches of epithelial crypts and ganglia. They also acquire a transcriptomic profile similar to that of fetal intestinal macrophages and display tissue macrophage behaviors, such as recruitment to tissue injury. Using this model, we show that macrophages reduce glycolysis in mesenchymal cells and limit tissue growth without affecting tissue architecture, in contrast to the pro-growth effect of enteric neurons. In short, we engineered an intestinal tissue model populated with macrophages, and we suggest that resident macrophages contribute to the regulation of metabolism and growth of the developing intestine.

INTRODUCTION

The intestine harbors a range of macrophage subtypes in distinct spatial niches. Within the villi, they phagocytose contents of the lumen through the epithelium.^{1–3} At the base of the epithelium, crypt-associated macrophages regulate epithelial stemness and differentiation.^{4–6} External innervation and the enteric nervous system (ENS) collaborate with adjacent macrophages to regulate immune response and peristalsis.^{7–9} Intriguingly, the intestine is populated with macrophages early in the embryonic development, found as early as embryonic day 9.5 (E9.5) in mouse foregut, before the above niches are developed.¹⁰ Unlike our knowledge of intestinal macrophages in adult organisms, it is unknown whether they influence prenatal intestinal development.

In general, developmental roles of macrophages are less understood than their functions in cellular immunity and niche-specific homeostasis. Accumulating evidence in mice and *ex vivo* studies, however, suggests that they are indispensable for proper development of certain tissues. At an embryonic stage,

they have been shown to regulate the growth of kidney, development of pancreatic islet, and formation of coronary plexus and lymphatic vessels in developing heart.^{11–14} During postnatal development, they are required for proper mammary epithelial remodeling and brain development.^{15–18} Furthermore, macrophages regulate the metabolism of peripheral cells. They have been shown to regulate insulin-dependent glucose metabolism of adipocytes, and this mechanism seems to be abused by cancer cells to promote tumor growth.^{19–21} A growing list of findings deepen our understanding of macrophages' homeostatic functions throughout the body; however, much less is known about their role in development.

Our current understanding of macrophages stems from many model systems, each with strengths and weaknesses. Zebrafish is an excellent vertebrate model that provides high *in vivo* optical accessibility during the developmental stage; however, its gross anatomical structures differ much from those of human. Mice have closer anatomical and physiological resemblance to humans and have pioneered macrophage biology as a transgenic



model; however, the efficacies of techniques such as cell ablation are variable between different organs, likely due to heterogeneity of resident macrophages.²² Human cell culture such as immortalized cell lines and blood monocyte-macrophage culture has also been a useful tool to study fundamental cell biology; however, they are limited in their capacity to model cell state in native tissue environments. Now, as an extension to the two-dimensional cell culture, advancements in directed differentiation of pluripotent stem cells (PSCs) enable us to generate cell types and tissue-like multicellular constructs to model human biology *in vitro*. Versatility in manipulation and complexity of the tissue-like constructs, also known as organoids, should be particularly useful to model early human development where access to material is difficult or implausible.

Methods to derive embryonic-like intestinal organoid and macrophage from human PSCs have been described previously.^{23–26} Here, we first assembled the intestinal organoid with macrophages, recapitulating their migration in early development. During our characterization of this model, we identified the major source of colony-stimulating factor 1 (CSF1), a growth factor crucial for macrophage differentiation and survival, to be mesenchymal cells in both the fetal intestine and the organoid. Macrophages in the organoid then localized to known intestinal microanatomical niches in xenograft-matured organoids. They also acquired a transcriptional profile similar to that of fetal intestinal macrophages. Functionally, they phagocytosed luminal antigens and migrated to wounds upon injury. Finally, we utilized this model to study the function of macrophages in intestinal development. Our experiments show that macrophages regulate glucose metabolism in the developing intestinal organoid and further its growth.

RESULTS

Derivation of human intestinal organoids with macrophages

Embryonic macrophages begin to migrate and populate the organism early in development.^{10,27} We postulated that macrophages would migrate and populate the intestinal organoid most efficiently beyond a specific developmental time point; thus, we inquired as to when intestinal macrophages are first observable. In mice, AIF1⁺ macrophages were first observed in the mid-hindgut at E10.5, which approximately corresponds to 30 days post conception (day 30) in human development or Carnegie stage 13 (CS13)²⁸ (Figures S1A and 1A). In humans, we identified macrophages in a single-cell RNA-sequencing (scRNA-seq) dataset of day-47 fetal proximal intestine, the earliest dataset reported to date²⁹ (Figures 2B–2D and S1D). The results thus indicate that macrophages populate both the mouse and human intestine at an early embryonic stage. Based on these results, we estimated that the first macrophage occupation of the human intestine would start approximately at day 30.

Human intestinal organoids (HIOs) and macrophages were derived from human induced PSCs (hiPSCs) based on previously described methods with minor modifications.^{23,25,30} We used macrophage derivation, which recapitulates early embryonic macrophage ontogeny.²⁶ Day-21 to day-28 HIOs were used, which roughly corresponds to day 30 based on our previous esti-

mation taking the inner cell mass formation (~7 days since conception) into account. HIOs were co-cultured with the macrophages in a three-dimensional Matrigel droplet for 7 days, during which time macrophages in the periphery migrated into HIOs (Figures 1C–1F and S1F). HIOs with macrophages (HIO/Mac) were then transferred into a new Matrigel droplet and cultured in the absence of peripheral macrophages for 7 days (Figure 1B). As expected, CD14⁺/AIF1⁺ macrophages were present in HIO/Mac but not in HIO (Figures 1D and 1F). Furthermore, macrophages proliferated within the HIO just like embryonic tissue resident macrophages (Figures S1B and S1C). Similar to E15.5 mice, macrophages in the HIO either associated tightly with the epithelium or were found within the surrounding mesenchyme (Figure S1E). In this study, macrophages and HIOs from three and two hiPSC lines, respectively, were used. We note that the incorporation of macrophages into organoid was successful in all samples, and the number of macrophages incorporated was comparable in most cell lines we tested. However, we also observed that the number of incorporated macrophages was significantly higher with one certain cell line; thus, cell-line-to-cell-line or batch-to-batch variation is to be expected (Figures 1G and 2F).

Cellular composition of the intestinal organoid resembles fetal intestine

We first examined the cellular composition of the organoid. In the intestine, neurons of the ENS localize closely with macrophages and together regulate peristalsis and immune response.^{7–9} To increase the complexity of HIO/Mac for following characterizations and experiments, we also derived HIO/Mac with ENS (HIO/ENS/Mac) by incorporating hiPSC-derived vagal neural crest cells, precursors to ENS³⁰ (Figure 2A). We then performed scRNA-seq on HIO/ENS/Mac to compare to the day-47 fetal intestine dataset. Presumptive cell identities were assigned to unsupervised clusters based on known gene markers (Figures 2B and 2C). Like the fetal intestine, the organoid consisted of mesenchyme, epithelium, enteric neurons, glial-like progenitors, and macrophages. Unlike the fetal intestine, the organoid did not yet develop any distinct smooth muscle cells or endothelial cells. As expected, the organoid lacked lymphocytes and erythroblasts (Figures 1B and 1C). A more detailed look at the cellular proportions indicated that although the organoid was more abundant in mesenchymal cells, the ratio of epithelial-to-mesenchyme and glial/progenitor-to-enteric neuron were comparable to those in fetal intestine, whereas the proportion of the neural cells and macrophages were lower in comparison with fetal intestine (Figure 1D). Cell-type identity was more directly compared between the fetal intestine and the organoid by merging the dataset and performing unsupervised clustering. Lymphocytes and erythroblasts were only present in the fetal intestine as expected, whereas smooth-muscle-like cells and endothelial-like cells were identified in the organoid. This likely indicates the potential for mesenchymal cells to differentiate into smooth muscle cells and endothelium as previously demonstrated in grafted organoids and vascular endothelial growth factor-treated HIOs, respectively.^{31,32} Together, the results indicate that our organoid model consists of expected cell types and proportions found in an early embryonic intestine.

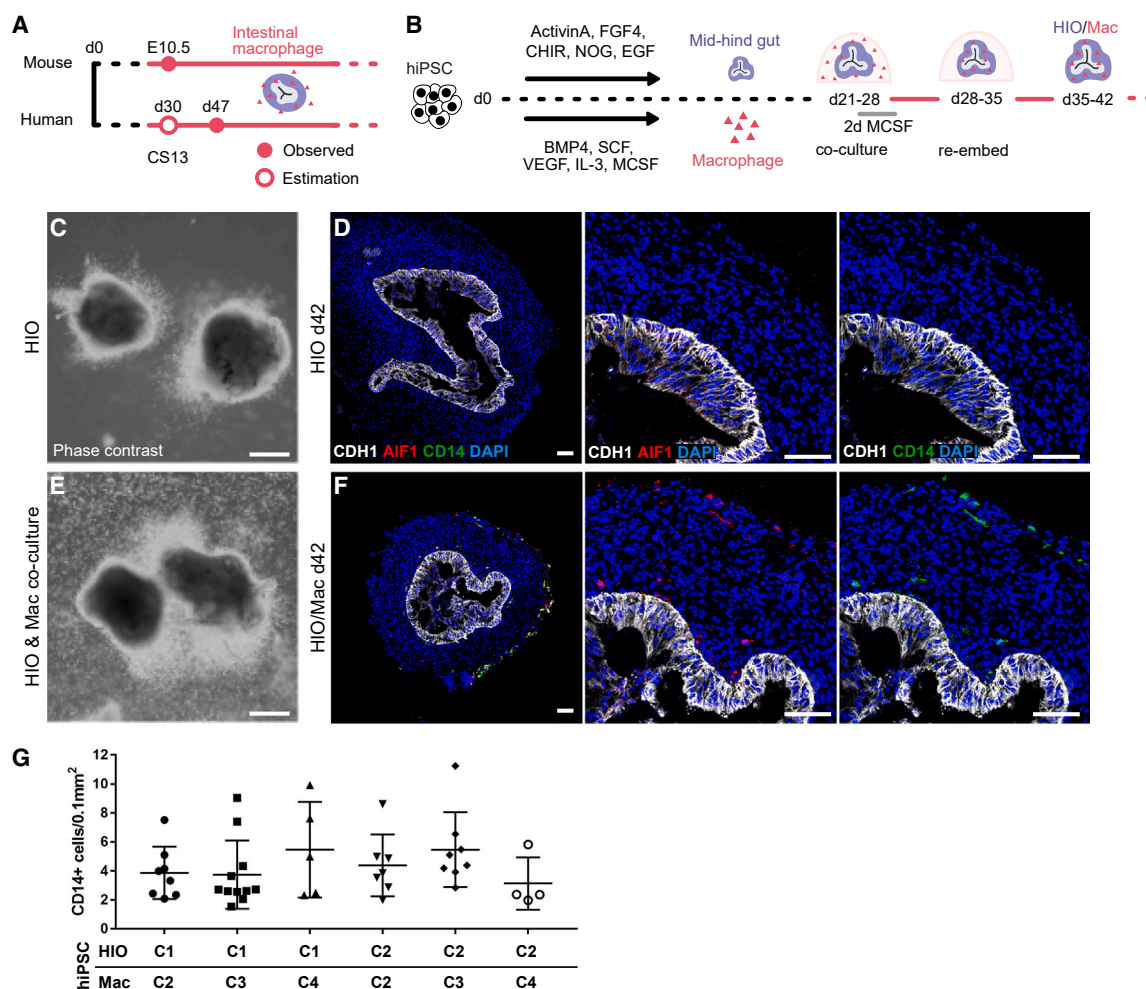


Figure 1. Derivation of human intestinal organoid with macrophages

(A) Timeline of macrophage habitation of mid-hindgut in mouse and human. d, days post conception; E, embryonic day; CS, Carnegie stage. See also Figure S1. (B) Overview of the derivation of human intestinal organoid with macrophages (HIO/Mac). hiPSC, human induced pluripotent stem cells; CHIR, CHIR99021.

(C and E) Phase-contrast image of day-28 HIO alone (C) or HIO in co-culture with hiPSC-derived macrophages (Mac) (E). Arrowhead points to HIO. Scale bars, 0.5 mm.

(D and F) Immunofluorescence of HIO and HIO/Mac for markers of epithelium (CDH1), macrophage (AIF1, CD14), and nucleus (DAPI). Scale bars, 75 μ m.

(G) Efficiency of macrophage incorporation into HIO with different iPSC lines (C1–C4, see STAR Methods). Number of Cd14-positive macrophages counted in non-epithelial region of the organoid (CDH1-negative and DAPI-positive) cryosections. HIO or macrophages derived from HIO/Mac are, for example, C1/C2 = HIO derived from C1 and macrophages derived from C2. Each data point represents an organoid. Data are mean and SD; p = 0.4274, one-way ANOVA.

Macrophage recruitment and retention by the organoid

CSF1 (macrophage colony-stimulating factor [MCSF]) is a crucial regulator of macrophage differentiation, survival, and proliferation, which is present in circulation and produced locally in tissues.^{33,34} It is unclear which specific cell types produce CSF1 in the developing intestine. Since macrophages occupied the area deep within the organoid and proliferated, we suspected that HIO produced CSF1. Single-cell datasets revealed that mesenchymal cells were the major cell type expressing CSF1 in both the organoid and day-47 to day-127 fetal intestine. CSF1 was also expressed in lymphocytes (T and natural killer) and endothelial cells in the fetal intestine, although these cells represented a much smaller proportion of CSF1-expressing cells (Figure S2A). We have previously supplemented the medium

with 100 ng/mL of MCSF; however, the above results suggested that the macrophages may not constantly require external MCSF. Indeed, we found that 20 ng/mL MCSF during the first 2 days of the co-culture was sufficient to derive HIO/Mac and that the addition of MCSF was not required for further culture (Figure 1B). In conclusion, we identify mesenchymal cells as the major producer of CSF1 in the developing intestine, which is recapitulated in the organoid, and find that this local production is sufficient to maintain the macrophage population in the organoid.

Next, we sought to further understand signaling pathways between macrophages and the organoid, since pathological levels of inflammatory signaling could be recruiting the macrophages to the organoid. To this end, we first looked at a curated list of

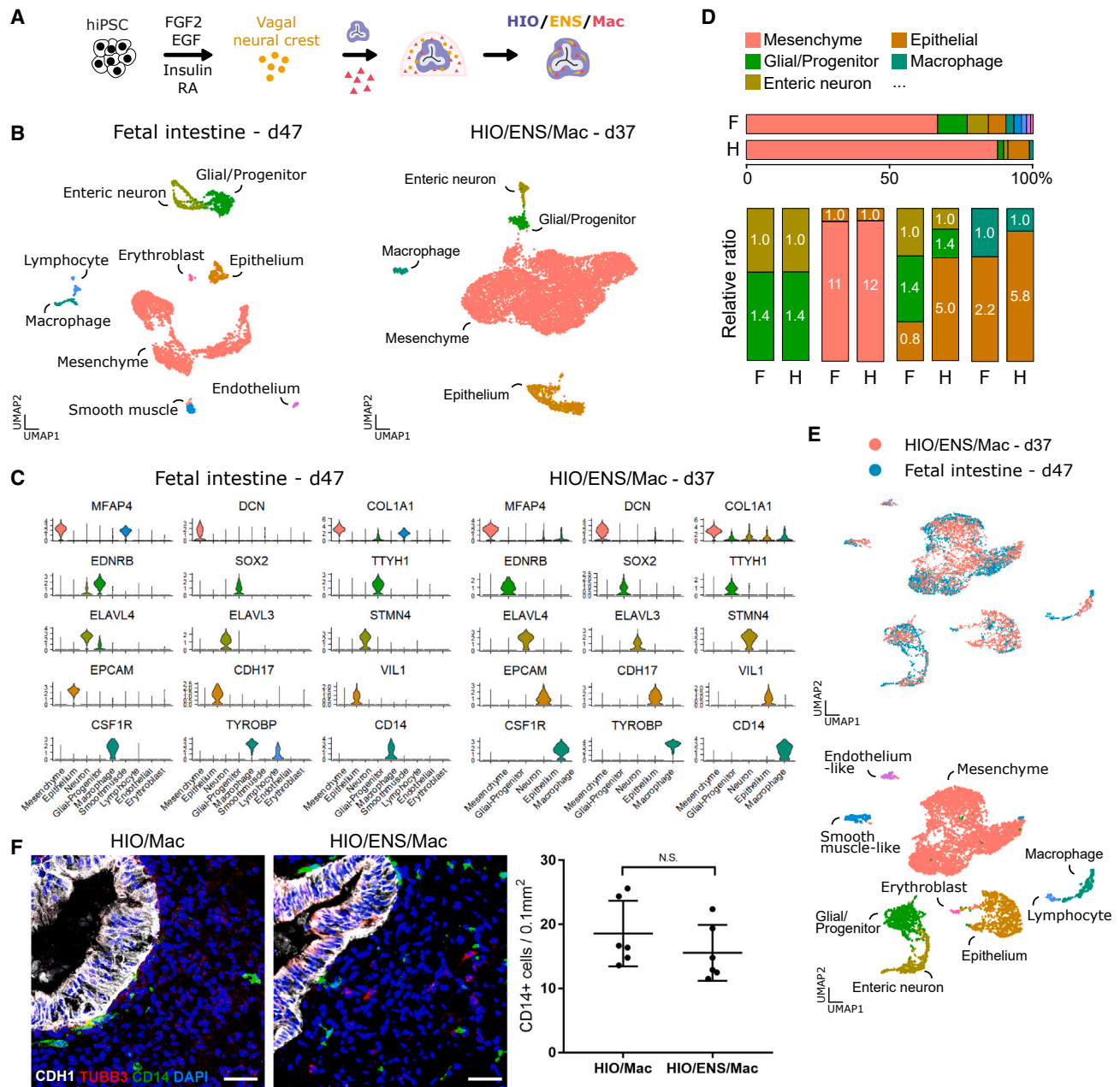


Figure 2. Cellular composition of human intestinal organoid with macrophages and enteric neurons

(A) Schematic of the derivation of HIO with enteric nervous system (ENS) and macrophages (HIO/ENS/Mac).

(B) Uniform manifold approximation and projection (UMAP) plot of single-cell RNA sequencing (scRNA-seq) of day-47 human fetal proximal intestine and day-37 HIO/ENS/Mac (C1/C2/C5).

(C) Violin plots of a representative gene used to identify the cell type of each cluster in UMAP from (B).

(D) Relative ratio of cell types in comparison of each dataset from (B).

(E) UMAP plot of merged dataset of day-47 human fetal proximal intestine and day-37 HIO/ENS/Mac.

(F) Immunofluorescence of day-42 HIO co-cultured only with macrophage or with macrophage and vagal neural crest cells (ENS precursor). Epithelium (CDH1), Neuron (TUBB3), macrophage (CD14), nuclei (DAPI), and the quantification of macrophage numbers within the HIOs. CD14-positive macrophages counted in non-epithelial region of the organoid (CDH1-negative and DAPI-positive) cryosections. Each data point represents an organoid. Result of two experiments. iPSC lines: HIO = C1, ENS precursor = C1 or C2, macrophage = C3 or C2. See also Figure S2G. n = 6 each. Data are mean and SD; p = 0.2996 (not significant [NS]), Student's t test. Scale bar, 45 μ m.

ligands upregulated during inflammation that promotes macrophage recruitment. These genes showed little to no mutual expression in the HIO cells and macrophages. On the other hand, *CX3CR1-CX3CL1* and *CSF1-CSF1R*, which are known effectors of macrophage recruitment and/or survival during development, showed high mutual expression (Figure S3A).^{35–37} Receptor expression levels in macrophages, which were co-cultured with the HIO, were validated with quantitative PCR (qPCR) against cells known to express receptor levels (Figures S2B and S2C). In conclusion, we show that the chemotactic signal gene expression between the organoid and the macrophage is not reminiscent of pathological inflammation but includes signaling involved in macrophage recruitment in development.

Enteric neurons do not affect resident macrophage establishment

A previous report suggests that enteric neurons are the main source of CSF1 in the muscularis of adult mouse intestine.⁹ On the other hand, during development, we observed little *CSF1* expression in enteric neurons of the organoid and day-47 to day-127 fetal intestine (Figure S2A). To test directly whether enteric neurons affect macrophage establishment in the developing intestinal organoid, we derived HIO combined with macrophages either with or without vagal neural crest cells. Presence of enteric neurons within the HIO did not affect the number of macrophages in the HIO (Figure 2F). This observation supports a previous report that the lack of enteric neurons in neonatal *Ret*^{−/−} mice and children with Hirschsprung's disease does not affect the establishment of intestinal macrophages.¹⁰ In conclusion, our results support the notion that enteric neurons do not affect macrophage colonization in early developing intestine.

Macrophages migrate to the wound site upon injury

We wanted to test whether macrophages in the organoid displayed behaviors of *in vivo* macrophages. One of the characteristic behaviors of macrophages is their recruitment to tissue injury, also observable during embryonic development.^{38,39} To test whether organoid macrophages can migrate to the injury site, we derived macrophages from eGFP-tagged hiPSCs (hiPSC^{eGFP}) and tracked their movements within the organoid after a puncture injury. Macrophages migrated toward the injury site during the 12 h following the injury, whereas the movements of macrophages in the uninjured organoids were not concerted. Assessment of their relative distance to the injury and the chemotactic precision index, which quantifies directional movement, supported this observation (Figures S2D–S2F). In conclusion, we show that macrophages in the early-stage *in vitro* organoid display recruitment behavior upon injury, as observed in developing mice.

Macrophages localize to intestinal microanatomical niches in xenograft-matured organoids

Macrophages localize to specific microanatomical niches within the intestine, such as villi, crypts, and enteric ganglia.^{4,5,7–9,40} To test whether macrophages in HIOs localize to these niches, we grafted HIO/ENS/Macs to immunodeficient *non-obese diabetic/Prkdc*^{SCID}/*Il2rg*^{null} (NSG) mice for 8–12 weeks to facilitate

further development, forming more complex tissue structures³¹ (Figure 3A). Furthermore, macrophages were derived from an hiPSC^{eGFP} line to trace their origin. The grafted organoids maintained CDX2⁺ intestinal epithelial identity and developed crypts, villi, smooth muscle, enteric ganglia, and glia.⁴¹ More so, the eGFP⁺ macrophages were observed in microanatomical niches of grafted organoids (Figures 3B–3D, S3A, and S3B).

In more detail, at the epithelium macrophages were positioned flat against the MKI67⁺CDH1⁺ epithelial crypt cells and congregated within the villi, comparable to the distribution and morphology seen in day-119 human fetal intestinal macrophages and in mouse⁸ (Figure 3C). Intestinal monocytes/macrophages near the epithelium phagocytose luminal content, such as bacteria.^{1–3} To test whether macrophages in the organoid display such transepithelial phagocytic activity, we injected *Escherichia coli* particles conjugated to pH-sensitive fluorescent dye into the lumen of grafted HIO/Mac^{eGFP}. Confocal microscopy images showed that eGFP⁺ macrophages near the epithelium internalized the particles, indicating transepithelial phagocytic activity (Figure S3D). In adult mice, intestinal macrophages were shown to regulate epithelial repair and intestinal stem cell niche.^{4–6} In particular, macrophage ablation was shown to decrease the number of MKI67⁺ (KI67, a cell-cycle marker) crypt cells.⁵ To test whether macrophages affect the crypt during development, we grafted HIO/ENS and HIO/ENS/Mac for comparison. Intriguingly, the number of cells in the cell cycle in the epithelium was lower without the macrophages. However, the epithelium was not longer in the organoids with macrophages (Figure S3E). We also note here that GFP[−]/AIF1⁺ macrophages were found in both HIO/ENS and HIO/ENS/Mac, indicating that macrophages from the NSG mice populated the grafted organoids (Figure S4C). Previous reports indicate that macrophages of NSG mice display a delay in maturation and defects in immune function but are unclear as to whether their homeostatic capacities are affected.^{42–46} Regarding our grafted experiments, hiPSC-derived human macrophages seem to exert an effect post grafting that NSG mouse macrophages do not. In conclusion, grafted organoids recapitulate macrophage localization in the intestinal mucosa and their transepithelial phagocytosis. Furthermore, hiPSC-derived macrophages increase the number of MKI67⁺ crypt cells in the developing organoid, similar to the previous reports in adult mice, but without affecting epithelial length.

At the enteric ganglia, organoid macrophages localized adjacent to the ELAVL4⁺ TUBB3⁺ neurons, resembling neuron-associated intestinal macrophages in day-119 human fetal intestine and adult mice^{8,9} (Figure 3D). The neurons in the ganglia also expressed enteric neuronal marker PHOX2B and associated with S100B⁺ glial cells (Figure S3B). Cell-ablation studies in adult mice indicate that macrophages regulate intestinal peristalsis.^{8,9} Grafted organoids undergo spontaneous peristalsis-like contractions. To test whether macrophages affect organoid peristalsis, we recorded the isometric force generated by whole grafted organoids with or without macrophages. However, we did not observe differences in contractility between the two conditions (Figure S3F). In conclusion, macrophages in the organoid associated with enteric ganglia as observed in the fetal and adult mouse intestine, but this physical association may not affect peristalsis during embryonic development.

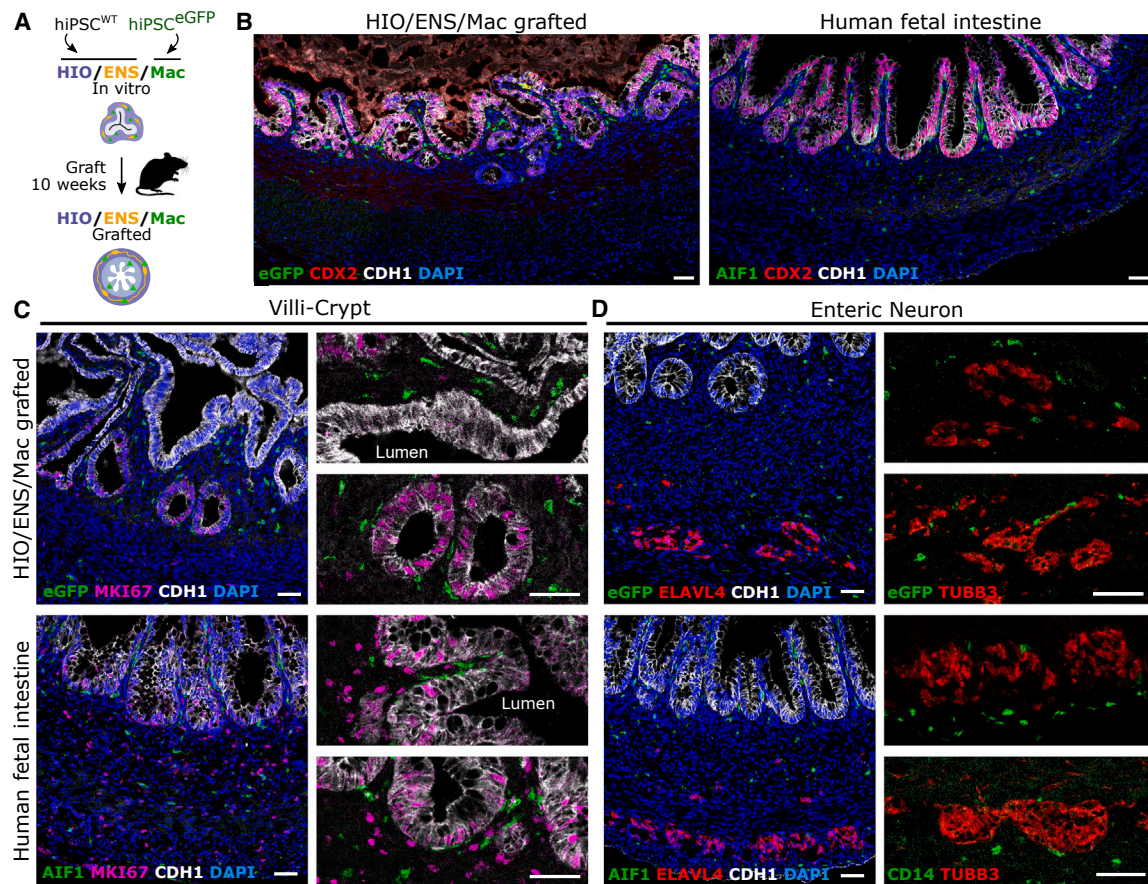


Figure 3. Macrophages localize to intestinal microanatomical niches in xenograft-matured intestinal organoid

(A) Strategy to track macrophages by deriving it from eGFP-tagged hiPSC (hiPSC^{eGFP}) and further differentiation and growth of the organoids by engrafting to the immunodeficient (NSG) mice.

(B) Representative immunofluorescence confocal microscopy images of day-112 grafted HIO/ENS/Mac (C1/C2/C4) and day-119 human fetal proximal intestine for intestinal epithelium specific identity (CDX2, CDH1) and macrophages (eGFP or AIF1).

(C) Localization of macrophages (eGFP or AIF1) within the villi (CDH1) and to crypts (MKI67, CDH1). Localization of macrophages with enteric ganglia (TUBB3, ELAVL4).

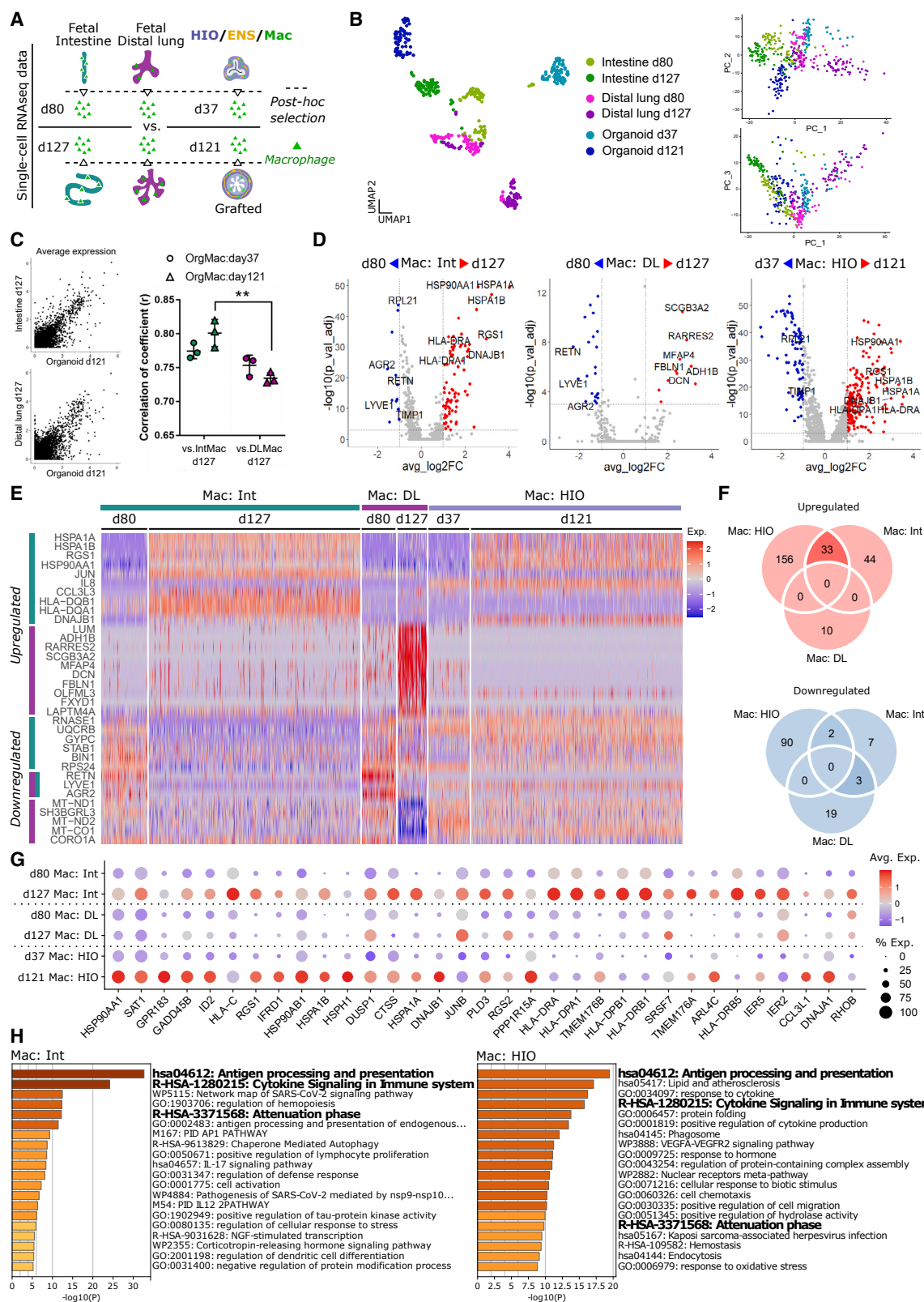
Nuclei (DAPI). Scale bars, 50 μ m.

Organoid macrophages acquire a transcriptomic profile like that of fetal intestinal macrophages

Macrophages/monocytes migrate into each organ and further differentiate to fulfill the locale-specific function.^{8,35,47} Similarly, previous *in vitro* experiments using murine iPSC-derived embryonic-like macrophages were shown to take on a microglia-like transcriptomic profile when co-cultured with neurons.⁴⁸ To find out whether organoid macrophages differentiate in response to their tissue environment, we examined the single-cell transcriptomic changes of macrophages in early-stage (*in vitro* day 37) organoid to later-stage organoid (grafted day 121). The organoid macrophages were also compared to human fetal intestinal macrophages and fetal distal lung macrophages, where the two served as the *in vivo* counterpart of similarity and dissimilarity.^{29,49} In detail, macrophages were subset from day 80 and day 127 of the fetal proximal intestine and distal lung datasets, and for day-37 *in vitro* organoid and day-121 grafted HIO/ENS/Mac^{eGFP} datasets. Macrophage clusters

from the unsupervised clustering of each dataset were further selected for *CSF1R*- and *CD14*-expressing cells (Figure 4A; see STAR Methods).

Unsupervised clustering of the datasets showed that earlier-stage (day 80) fetal macrophages were still similar to each other, although early-stage (day 47) organoid macrophages were less similar to the fetal macrophages. Later-stage (day 127) fetal macrophages diverged away from each other, and later-stage (day 121) organoid macrophages diverged closer to the later-stage intestinal macrophages (Figure 4B). Additionally, principal component analysis showed that later-stage organoid macrophages diverged away from earlier-stage macrophages in similar dimension as later-stage fetal intestinal macrophages (Figure 4B). To quantify this observation at large, we calculated the correlation of coefficient between the different macrophages. The correlation was higher between intestinal and organoid macrophages compared to lung and organoid macrophages (Figure 4C).



(legend on next page)

To see which specific changes each macrophage undergoes, we analyzed differentially expressed genes between the later and earlier time points of each macrophage. Each fetal macrophage showed distinct gene upregulation. Intestinal macrophages increased antigen-presentation-related gene expression (HSPs, HLAs, *TMEM176A*, *TMEM176B*), whereas distal lung macrophages upregulated genes that were previously known to regulate lung morphogenesis (*SCGB3A2*, *ADH1B*, *RARRES2*) and extracellular matrix protein enriched in the lung (*FBLN1*)^{50–55} (Figure 4E).

Differentially regulated profiles were then compared to that of organoid macrophages. A heatmap of the top ten differentially expressed genes from intestinal and distal lung macrophages demonstrated that organoid macrophages shared upregulated genes with intestinal but not with distal lung macrophages (Figure 4F). Specifically, 33 out of 77 upregulated genes were shared between intestinal and organoid macrophages, with significant enrichment of “Antigen processing and presentation” in intestinal and organoid macrophages (Figures 4G, 4H, and S4A). Genes only upregulated in intestinal macrophages included additional HLA genes (Figures S4A and S4B). Gene set enrichment analysis (GSEA) also showed enrichment in antigen-presentation terminologies (Figure S4C). Comparisons of additional fetal intestinal datasets with varying developmental intervals showed similar signature where antigen-presentation genes are upregulated (Figure S4D). Downregulation profiles between intestinal and distal lung macrophages were less discernible (Figures 4F and 4G). In conclusion, we find that macrophages in the organoid undergo tissue specification similar to that of the fetal intestine at a transcriptional level.

Macrophages regulate intestinal organoid growth

Intriguingly, HIO/ENS engrafted for 10 weeks in the NSG mice were smaller when iPSC-derived macrophages were incorporated (Figures 5A–5C). Organoids used for the co-culture with macrophages were randomized during their derivation and their size shortly after the macrophage co-culture was still comparable (Figure 5G). Histology did not show differences in tissue morphology between the two conditions in 10-week grafted organoids. We argued that if the macrophages induced a chronic pro-inflammatory effect, they can cause abnormal fibrosis due to prolonged inflammatory state and in turn stunt growth; however, we did not observe any signs of abnormal fibrosis or tissue architecture on histology (Figures 5A and 5B). Additional organoids

with macrophages that were grafted for 8 weeks and 12 weeks were also smaller compared to organoids without macrophages (Figures 5C and 5E). Exponential fit of the organoid size as function of time indicated that the rate of growth was reduced when incorporated with macrophages (Figure 5D).

Macrophages are professional phagocytes; thus, we next tested whether the reduction in size of grafted organoids by the macrophages is due to the removal of apoptotic cells. Levels of immunofluorescence signal for apoptotic cells, however, were comparable between the grafted organoids with or without macrophages (Figure 5F). Thus, the size difference is not due to the removal or accumulation of apoptotic cells.

In the report that described the HIO/ENS derivation, bulk RNA-seq showed that organoids combined with ENS had higher epidermal growth factor expression, although size difference was not noted.³⁰ Additionally, macrophages in the brain (microglia) were shown to phagocytose neuronal processes and were required for proper brain development and morphology.^{17,18} Thus, intestinal macrophages may suppress overt expansion of enteric neurons and in turn inhibit tissue overgrowth. We hypothesized that the reduced growth of organoids by macrophages is dependent on the presence of ENS. Comparison between grafted HIO and HIO/ENS showed that ENS did have a positive growth effect; however, reduced organoid growth by macrophages was independent of ENS (Figures 5G and 5H). We conclude that ENS and macrophages regulate organoid growth in a positive and negative manner, respectively, and that neither of the effects is necessarily dependent on one another.

Macrophages attenuate mesenchymal cell glycolysis in developing intestinal organoids

To further investigate the roles of macrophages in early intestinal development, we performed scRNA-seq on organoids with or without macrophages (two HIO/ENS pairs and one HIO pair) and looked at the transcriptomic differences between each cell type (Figure 6A). Differentially expressed genes common in all three sample pairs were found in the mesenchyme and the epithelium (Figure 6B). The most discernible gene ontology annotation among these results was the downregulation of key glycolytic enzymes (*ENO1*, *LDHA*, *PFKP*, *PGK1*, and *TPI1*) in mesenchyme, suggesting a decrease in their glycolysis when macrophages are present (Figures 6C and 6E). GSEA also showed similar results (Figures S5B and S5C). Macrophages

Figure 4. Intestinal organoid macrophages acquire transcriptomic profile like that of fetal intestinal macrophages

- (A) Overview of post hoc selection process for macrophages from organoid and fetal tissue scRNA-seq datasets. *In vitro* HIO/ENS/Mac (C1/C2/C5). Grafted HIO/ENS/Mac (C1/C1/C4).
- (B) UMAP plot of early- and late-stage fetal and organoid macrophages (left) and principal component analyses of the same (right).
- (C) Representative scatterplots of average gene expression between fetal and organoid macrophages. Pearson's correlation of coefficient (r) of the average gene expression comparisons. Data are mean and SD. $p = 0.0082$. Student's t test was performed on Z scores, calculated from r values using Fisher's transformation.
- (D) Volcano plots of differentially expressed genes in the macrophages between late and early developmental time points. Threshold of discovery (dotted line), \log_2 fold change >1 , adjusted p value <0.001 , Wilcoxon rank-sum test. Mac, macrophage; Int, intestine; DL, distal lung.
- (E) Heatmap of top ten upregulated and downregulated genes of the late vs. early fetal proximal intestine, and distal lung in the order of fold change. Number of cells in “Mac: HIO” were downsampled for visualization. Exp, scaled expression level.
- (F) Venn diagram of the number of upregulated and downregulated genes from (D).
- (G) Dot plot of the 33 commonly upregulated genes between intestinal and organoid macrophages. Avg. Exp, average expression; % Exp, percentage of cells expressing the gene.
- (H) Gene ontology annotation of intestinal and organoid macrophages generated with all the upregulated genes for each dataset.

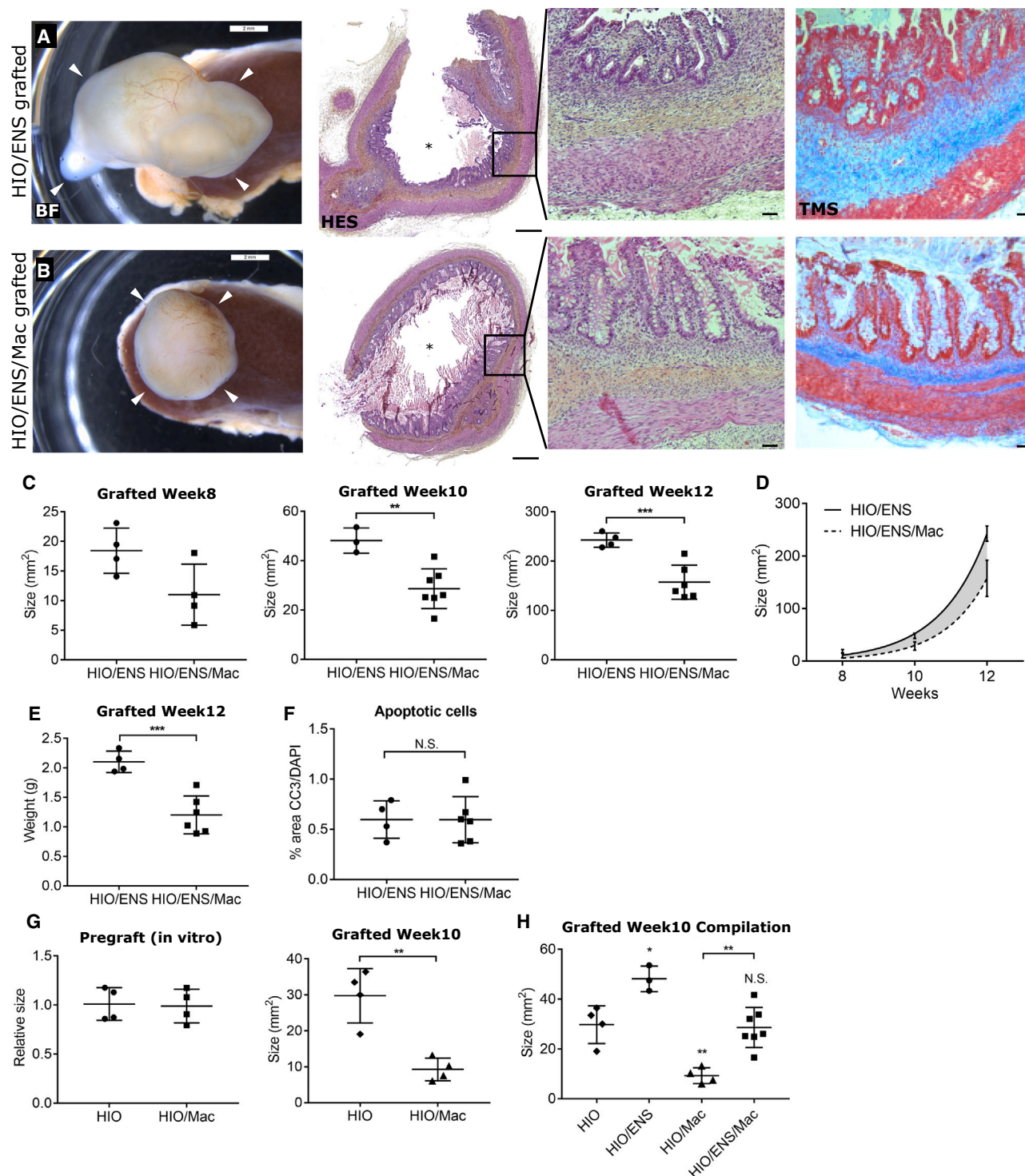


Figure 5. Macrophages reduce the growth of intestinal organoid without affecting tissue architecture

(A and B) Representative bright-field images of week-10 grafted organoids still attached to the mouse kidney at the site of the engraftment, White arrowheads point to the organoid. Hematoxylin-eosin-saffron (HES)-stained sections of the grafted organoids. Trichrome Masson (TMS)-stained sections. Asterisks indicate lumen. Scale bars, 2 mm (BF), 0.4 mm (HES), and 50 μ m (HES and TMS insets).
(C) Size measured by the area of the grafted organoids from bright-field images, isolated at 8 weeks, 10 weeks, and 12 weeks after the engraftment. Week 8: HIO/ENS (C1/C2), n = 4; HIO/ENS/Mac (C1/C2/C5), n = 4; p = 0.0633. Week 10: HIO/ENS (C1/C2), n = 3; HIO/ENS/Mac (C1/C2/C5), n = 7; p = 0.0034. Week 12: HIO/ENS (C1/C2), n = 4; HIO/ENS/Mac (C1/C2/C3), n = 6; p = 0.0010. Welch's t test.

(legend continued on next page)

were previously shown to regulate glucose uptake and metabolic response to cold in adipocytes.^{20,21} They were also shown to upregulate glycolysis in cancer cells and promote tumor growth.¹⁹ Mapping protein-protein association of the downregulated mesenchymal genes revealed a network of the aforementioned glycolytic genes as expected, but also their associations with *MIF* (Figure 6D). *MIF* was previously shown to promote glucose uptake and glycolysis of muscle and cancer cells, and was shown to be expressed in intestinal epithelium.^{56–58} *MIF* was also downregulated in the organoid epithelium (Figure 6E). In conclusion, organoid macrophages reduced the expression of glycolytic genes of the organoid mesenchymal cells.

We used the metabolic-flux assay (Seahorse XF) to test whether macrophages downregulate glycolysis in HIO's mesenchymal cells as indicated by the scRNA-seq result. Mesenchymal cells were dissected and isolated into single-cell suspension from either HIO or HIO/Mac. Macrophages were removed from the cell suspension with anti-CD14 antibody-mediated magnetic separation (Figure S5A; see STAR Methods). The extracellular acidification rate (ECAR) of the mesenchymal cells was measured to gauge their glycolytic activity (Figure 6F). Non-glycolytic acidification in the glucose-depleted state showed comparable ECAR between the two conditions. Introduction of glucose induced an increase in ECAR in both conditions as expected; however, mesenchymal cells from HIO/Mac showed a smaller increase, indicating a lower level of glycolysis. Subsequent inhibition of mitochondrial respiration with oligomycin, necessitating the cells to use glycolysis-driven ATP generation, showed that the glycolytic capacity was also lower in mesenchymal cells from HIO/Mac. Lastly, inhibition of glucose uptake by 2-deoxy-D-glucose decreased the ECAR again to a comparable level (Figure 6G). Thus, the metabolic-flux assay supports our transcriptomic result that macrophages reduce the glycolysis of mesenchymal cells.

Oncostatin M reduces key glycolytic gene expression in mesenchymal cells

We next looked at which signaling pathway may be involved in the glycolytic regulation by macrophages. Upon inquiring the ligand-receptor repository, we found an oncostatin M (OSM)-leukemia inhibitory factor receptor (LIFR) pathway between macrophages and mesenchyme in the organoid. OSM and two of its receptors, LIFR and OSMR, were also expressed (Figure 7A).⁵⁹ OSMR was also expressed in organoid mesenchymal cells. Additionally, a small population of fetal intestinal macrophages also expressed OSM and the two receptors in the

respective cell types (Figure S6). Previous reports show that dysregulation of the OSM pathway causes disruption of glucose homeostasis.^{60–63} Thus, we hypothesized that OSMs produced by organoid macrophages are involved in the downregulation of glycolysis in the mesenchymal cells. Mesenchymal cells were isolated from HIO and treated with OSM (Figure 7B). In response to the OSM treatment, mesenchymal cells showed downregulation of three out of five glycolytic genes (*ENO1*, *PFKFB*, and *PGK1*) identified in the scRNA-seq experiment (Figures 7C and 6A–6E). In conclusion, the results suggest that OSM from macrophages is a part of the signaling involved in negatively regulating glycolytic gene expression in mesenchymal cells in the developing organoid (Figure 7D).

DISCUSSION

Here, we studied the effect of macrophages on human intestinal development by engineering and utilizing a PSC-derived intestinal tissue model with macrophages. We describe an efficient and reproducible means of deriving HIO with macrophages (HIO/Mac) in which the macrophages localized to known micro-anatomical intestinal niches and acquired a transcriptional profile similar to that of fetal intestinal macrophages. Our approach improves the complexity of HIOs and improves on a previously published approach by providing tissue architecture with physiologically relevant macrophage distribution, higher reproducibility, and developmental relevance.⁶⁴ Functionally, macrophages in our HIO/Mac model phagocytosed luminal antigens and migrated to wounds upon injury. Most importantly, we demonstrate that macrophages regulate the metabolism and organ growth of the developing intestinal organoid.

We identified mesenchymal cells to be the major producer of CSF1 in the early developing intestine and organoid. A previous study in E17.5 mice has identified endothelial and interstitial cells of Cajal (ICCs) to have significant *Csf1* expression.¹⁰ Our single-cell analyses on human fetal intestine (days 47, 85, and 127) and organoid (day 37) also observed expression of *CSF1* in both endothelial and ICCs; however, the relative expression level, percentage of expressing cells, and percentage of expressing cells within the intestine was not comparable to those of mesenchymal cells. Thus, we conclude that mesenchymal cells are quantitatively the major source of CSF1 during early human intestinal development.

Macrophages are required for proper regeneration in the adult.^{38,65} Scarless wound healing in the fetus can be an intriguing avenue for the study of mammalian wound healing.

(D) Exponential regression of the size of the grafted organoids over time from (C). $p < 0.0001$, two-way ANOVA.

(E) Weight of 12-week grafted organoids from (C). $p = 0.0005$, Welch's *t* test.

(F) Level of apoptosis in grafted organoids. Quantified by calculating the area of cleaved caspase 3 (CC3) divided by the area of nuclei (DAPI) in confocal microscopy images of immunofluorescence. HIO/ENS, $n = 4$; HIO/ENS/Mac, $n = 6$. $p = 0.995$, Welch's *t* test.

(G) Relative size of HIO and HIO/Mac *in vitro* 2 weeks after the combination procedure and the size of the same organoids after a 10-week engraftment. HIO (C1), $n = 4$; HIO/Mac (C1/C3), $n = 4$. $p = 0.8625$, $p = 0.0075$, Welch's *t* test.

(H) Sizes of all 10-week grafted organoids combined with or without ENS precursors and/or macrophages. $p < 0.0001$, one-way ANOVA; HIO vs. HIO/ENS, $p = 0.0148$; HIO vs. HIO/Mac, $p = 0.0038$; HIO vs. HIO/ENS/Mac, $p = 0.9930$; HIO/ENS vs. HIO/Mac, $p < 0.0001$; HIO/ENS vs. HIO/ENS/Mac, $p = 0.0045$; HIO/Mac vs. HIO/ENS/Mac, $p = 0.002$; post hoc Tukey.

Each data point represents an organoid. Results from three experiments. Batch 1: week 8 and week 10 (C). Batch 2: week 12 (C, E). Batch 3: week 10 (G). Data in all graphs are mean and SD.

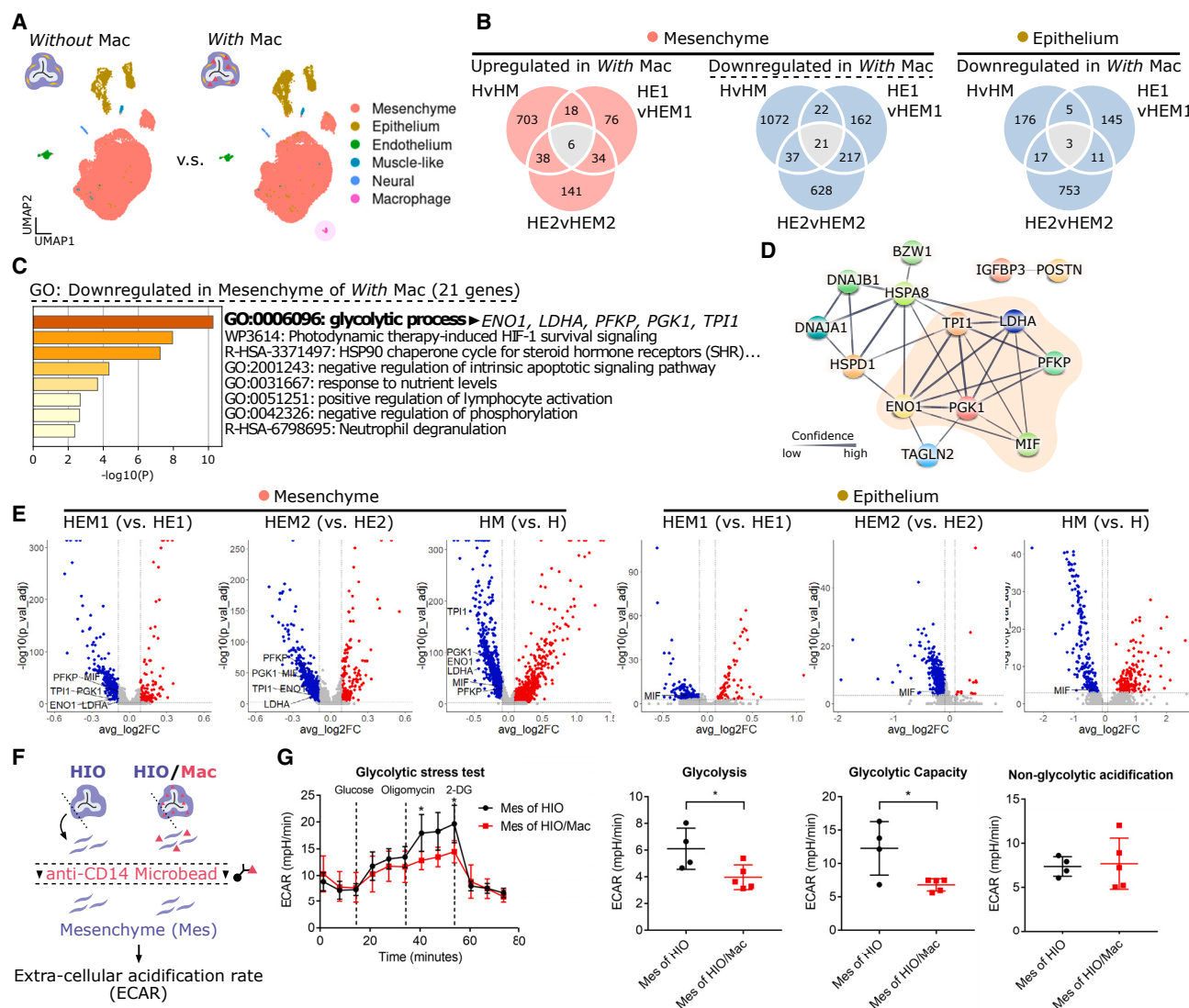


Figure 6. Macrophages attenuate mesenchymal cell glycolysis in developing intestinal organoids

(A) Representative UMAP plots from scRNA-seq datasets of *in vitro* organoids without and with macrophages (Mac). Merged dataset of HIO/ENSs and HIO/ENS/Macs.

(B) Venn diagram of the number of differentially expressed genes in organoids with macrophages against organoids without macrophages between the three separate comparisons. Differentially expressed genes in common among the three were found in mesenchyme and epithelium. HvHM (HIO [C1] vs. HIO/Mac [C1/C4]); HEvHEM (HIO/ENS [C1/C1] vs. HIO/ENS/Mac [C1/C1/C4]). Each sample is a pool of 4–5 dissociated organoids. Threshold of discovery: adjusted p value < 0.001, log₂ fold change > 0.09 and < −0.09, Wilcoxon rank-sum test.

(C) Gene ontology analysis of the 21 genes downregulated in organoid mesenchymal cells by organoid macrophages from (B).

(D) Protein-protein association map of the 21 genes from (B) using STRING. Only the genes with at least one association are displayed.

(E) Volcano plots annotated with genes involved in glycolytic process found with gene ontology (C) and protein-protein association map (D). Dotted lines: adjusted p value < 0.001, log₂ fold change > 0.09 and < −0.09, Wilcoxon rank-sum test.

(F) Schematic of mesenchymal cell isolation from *in vitro* organoids (HIO [C1] and HIO/Mac [C1/C5]) for the glycolytic stress test.

(G) Extracellular acidification rate (ECAR) measurement in the glycolytic stress test. Oligomycin (ATP synthase inhibitor). 2-DG, 2-deoxy-D-glucose (competitive inhibitor of glucose). Quantification of glycolysis, glycolytic capacity, and non-glycolytic acidification from the glycolytic stress test. See STAR Methods for calculation. Result of one experiment. Data are mean and SD. Glycolytic stress test: p < 0.0001, two-way ANOVA; p = 0.0311, p = 0.0289, post hoc with Sidak-Bonferroni. Each data point represents a technical replicate well. Glycolysis: p = 0.0360; glycolytic capacity: p = 0.0199; non-glycolytic acidification: p = 0.8452; Student's t test.

Further adaptation of the method described here should be useful for exploring the mechanisms and limitations of wound healing and how macrophages react in fetal injury or infection.

A fetal cell atlas project previously noted that antigen-presenting macrophages were found mostly in the gastrointestinal tract.⁶⁶

We found that intestinal macrophages acquire this antigen-presenting profile over time, indicating that this functional characteristic is induced by intestinal environment rather than derived from the ontological origin of the embryonic macrophages. Furthermore, acquisition of the antigen-presenting profile of organoid

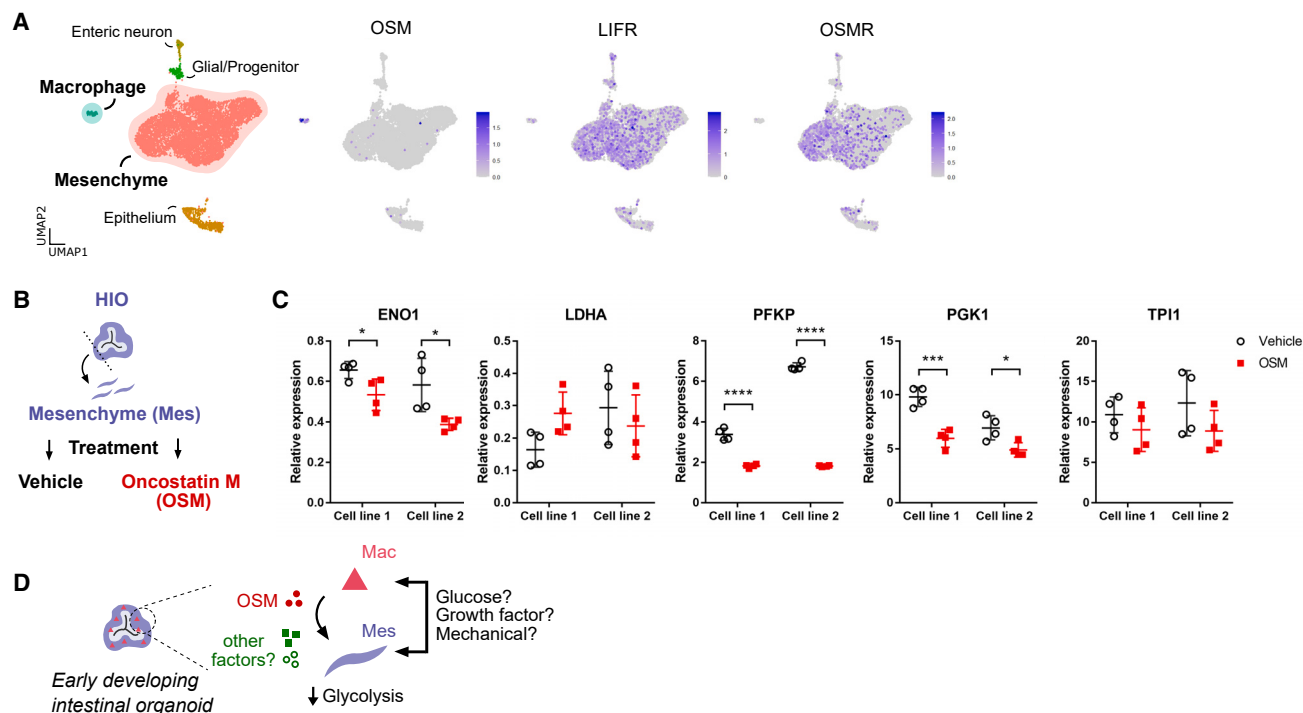


Figure 7. Oncostatin M reduces glycolytic gene expression in mesenchymal cells

(A) Expression of oncostatin M (OSM) and leukemia inhibitory factor receptor (LIFR) in the *in vitro* organoid (HIO/ENS/Mac [C1/C2/C5]) scRNA-seq dataset. (B) Schematic of mesenchymal cell isolation from *in vitro* organoids (C1 and C2) and treatment with either vehicle (0.1% BSA in PBS) or OSM (500 ng/mL). (C) Glycolytic gene expressions in OSM-treated mesenchymal cells by qPCR. Normalized to HPRT1 expression. Result of two independent experiments. Data are mean and SD. ENO1: $p = 0.0325$, $p = 0.0282$; LDHA: $p = 0.0392$, $p = 0.4785$; PFKP: $p < 0.0001$, $p < 0.0001$; PGK1: $p = 0.0008$, $p = 0.0199$; TPI1: $p = 0.3304$, $p = 0.1980$. (D) Schematic summary of macrophage's effect on the organoid's glycolysis. Mac, macrophage; Mes, mesenchyme.

macrophages suggests that HIO/Mac replicate this intestinal environment in this regard. It is intriguing to note that the organoids were kept in aseptic conditions during both *in vitro* culture and engraftment. Thus, the induction of the antigen-presentation profile in organoid macrophages, also observed in fetal intestine, occurred in the absence of microbiota. This suggests that intestinal tissue itself can induce the antigen-presentation profile of macrophages in the prenatal stage.

Our scRNA-seq analysis showed downregulation of glycolytic gene expression in the mesenchymal cells from organoids with macrophages. A subsequent ECAR experiment showed reduced glycolysis in these mesenchymal cells. We also found that OSM, expressed by macrophages, downregulated three of the five glycolytic genes from the scRNA-seq analysis. Our results suggest that macrophages can regulate the glucose metabolism of mesenchymal cells during intestinal development, in part involving OSM as the regulatory signal. Previous reports do indicate that they are required for proper regulation of glucose metabolism in adult mouse adipocytes, where catecholamines mediated the lipolytic activity of the brown adipocytes.^{20,21} OSM is also implicated in glucose homeostasis in adult mice, although the mechanism has not reached consensus.^{60–63} We suspect that metabolic regulatory functions of macrophages are already present at an early developmental stage. Metabolic dysregulations, such as hyperglycemia, negatively affect embry-

onic development.^{67–70} Thus, it is conceivable that mechanisms exist in early development to provide finer control over the embryo's local metabolism. Further investigation is required, including which environmental cues (e.g., glucose level) and which other regulatory signals (e.g., OSM, MIF) are present.

Unexpectedly, we find that later-stage grafted organoids with macrophages are smaller in size, suggesting that macrophages have an inhibitory role in the growth of a developing intestine. Neither fibrosis nor buildup of apoptotic cells seem to be the cause of the size difference. Our scRNA-seq and follow-up experiments show a decrease of glycolysis in mesenchymal cells of early-stage *in vitro* organoids with macrophages. We also find that OSM by macrophages are involved in the glycolytic downregulation of mesenchymal cells. LIFR, an OSM receptor, was previously shown to activate the Hippo pathway that negatively regulates organ growth.⁷¹ We did not find evidence to suggest that glycolytic metabolism causes an organ growth effect or vice versa; however, they may share the Hippo-related pathway as a common upstream regulator. Further investigation is required.

The number of MKI67 (a marker of the cell cycle)-positive cells in the epithelial crypt region was increased in the organoids combined with macrophages, seemingly contrary to the result of decreased overall size of the organoids. Furthermore, our quantification of the epithelial length showed no significant difference between two conditions, indicating that a higher proportion of

epithelial crypt was engaged in a cell-cycle state without contributing significantly to the overall epithelial growth. MKI67 is a graded-non-binary marker of proliferation, and intestinal stem cells seem to engage in a prolonged G₁ cell-cycle state.^{72,73} Thus, it is conceivable that more crypt cells are engaged in the cell cycle but that the number of cells committing to a proliferation remains unchanged. Furthermore, previous studies show that macrophage ablation in adult mice results in a decreased proportion of MKI67-positive crypt cells. In these ablations, however, they show a small decrease in the small intestine but also a significant increase in the villi/crypt length of the large intestine. These reports indicate that changes in MKI67-positive crypt cells do not necessarily correlate with epithelial length in this biological context.^{5,74} On a related note, potential differences between prenatal and postnatal intestinal stem cell niche behavior should also be considered in future investigations.⁷⁵

Modularity of the HIO/Mac, as demonstrated here by vagal neural crest cell or macrophage exclusion experiments, is particularly useful when cellular composition is an experimental variable. Similar cell-exclusion experiments should be useful to examine specific effects of embryonic macrophages in tissue development, such as their role on vascular and lymphatic development.^{9,13,14}

In conclusion, we engineered early intestinal tissue with macrophages from human PSCs in order to model the effect the macrophages on intestinal development. Our results provide an insight into potential macrophage function in embryonic development where they regulate metabolism and tissue growth. In addition, due to the relative simplicity of the derivation method and reproducibility, we expect the model to further facilitate the study of macrophage specifications and functions in development.

Limitations of the study

We utilized derivation of macrophages that is MYB-independent and thus yolk-sac-like in ontogeny.²⁶ From mice, we can deduce that yolk sac macrophages are the first to occupy the embryonic intestine, likely followed by fetal liver. It is still to be determined whether functional differences are present among embryonic macrophages dependent on the ontogeny of tissue macrophages, such as yolk sac vs. fetal liver vs. aorta-gonad mesonephros. Depletion and repopulation experiments in mouse lung suggest that functionality between the ontogenies is comparable.⁷⁶ However, if otherwise in the intestine, alternative macrophage derivation methods other than described here would have to be utilized to recapitulate the ontological differences. Additionally, there are mechanisms between macrophages and organoids that we could not identify here, namely, how macrophages regulate organoid size and whether glycolytic regulation by macrophages is associated with organoid growth. Sex-dependent effects were not explored in this study.

STAR★METHODS

Detailed methods are provided in the online version of this paper and include the following:

- KEY RESOURCES TABLE
- RESOURCE AVAILABILITY

- Lead contact
- Materials availability
- Data and code availability
- EXPERIMENTAL MODEL AND SUBJECT DETAILS
 - Cell lines and tissues
 - Mice
 - Pluripotent stem cell culture
- METHOD DETAILS
 - Human intestinal organoid derivation
 - Vagal neural crest derivation
 - Macrophage derivation
 - HIO combination with VNCC and macrophage
 - Human dendritic cell
 - Immunocytochemistry
 - Immunofluorescence and histology
 - Quantitative PCR
 - Grafting of organoids to immunodeficient mice
 - E.Coli particles injection into the grafted organoid lumen
 - Live imaging of injured HIO/Mac
 - Isometric force measurement
 - Single cell RNA sequencing and analysis
 - Glycolytic stress test
 - OSM treatment
- QUANTIFICATION AND STATISTICAL ANALYSIS

SUPPLEMENTAL INFORMATION

Supplemental information can be found online at <https://doi.org/10.1016/j.celrep.2023.113616>.

ACKNOWLEDGMENTS

We recognize and thank the following individuals and organizations. CHUSJ core facilities: reprogramming of cells and gene editing, Basma Benabdallah; cytometry, Ines Boufaied; imaging by microscopy, Elke Kuster. Sabine Herblot from the Michel Duval lab provided the human dendritic cells. The Sylvain Chemtob lab offered the use of isometric force measurement apparatus. A.S. was granted a scholarship from Fonds de Recherche du Québec Nature et Technologies. The project was supported by the Banque Nationale Research Excellence Chair in Cardiovascular Genetics held by G.A.

AUTHOR CONTRIBUTIONS

R.H.M.S., A.T.S., and S.L. derived the macrophages. Y.L. performed surgical procedures in mice. S.L. and P.P.v.V. prepared the libraries for scRNA-seq. A.T.S., H.A., and L.F. performed bioinformatics analyses. T.A. performed the glycolytic stress test. M.C. and A.T.S. performed image analyses. J.-V.G. and N.P. collected the fetal tissues. A.T.S. conducted the other experiments, designed the experiments, and wrote the paper with contributions from the co-authors. G.A. supervised all aspects of the study and provided funding.

DECLARATION OF INTERESTS

The authors declare no competing interests.

Received: October 25, 2023
Revised: November 22, 2023
Accepted: December 7, 2023

REFERENCES

- Niess, J.H., Brand, S., Gu, X., Landsman, L., Jung, S., McCormick, B.A., Vyas, J.M., Boes, M., Ploegh, H.L., Fox, J.G., et al. (2005). CX3CR1-Mediated Dendritic Cell Access to the Intestinal Lumen and Bacterial Clearance. *Science* (80–307), 254–258.
- Wang, J., Gusti, V., Saraswati, A., and Lo, D.D. (2011). Convergent and Divergent Development among M Cell Lineages in Mouse Mucosal Epithelium. *J. Immunol.* 187, 5277–5285.
- Lelouard, H., Fallet, M., de Bovis, B., Méresse, S., and Gorvel, J. (2012). Peyer's Patch Dendritic Cells Sample Antigens by Extending Dendrites Through M Cell-Specific Transcellular Pores. *Gastroenterology* 142, 592–601.e3.
- Cosín-Roger, J., Ortiz-Masiá, D., Calatayud, S., Hernández, C., Esplugues, J.V., and Barrachina, M.D. (2016). The activation of Wnt signaling by a STAT6-dependent macrophage phenotype promotes mucosal repair in murine IBD. *Mucosal Immunol.* 9, 986–998.
- Sehgal, A., Donaldson, D.S., Pridans, C., Sauter, K.A., Hume, D.A., and Mabbott, N.A. (2018). The role of CSF1R-dependent macrophages in control of the intestinal stem-cell niche. *Nat. Commun.* 9, 1272.
- Pull, S.L., Doherty, J.M., Mills, J.C., Gordon, J.I., and Stappenbeck, T.S. (2005). Activated macrophages are an adaptive element of the colonic epithelial progenitor niche necessary for regenerative responses to injury. *Proc. Natl. Acad. Sci.* 102, 99–104.
- Gabanyi, I., Muller, P.A., Feighery, L., Oliveira, T.Y., Costa-Pinto, F.A., and Mucida, D. (2016). Neuro-immune Interactions Drive Tissue Programming in Intestinal Macrophages. *Cell* 164, 378–391.
- De Schepper, S., Verheijden, S., Aguilera-Lizarraga, J., Viola, M.F., Boesmans, W., Stakenborg, N., Voytyuk, I., Smidt, I., Boeckx, B., Dierckx de Casterlé, I., et al. (2018). Self-Maintaining Gut Macrophages Are Essential for Intestinal Homeostasis. *Cell*, 1–16.
- Muller, P.A., Koscsó, B., Rajani, G.M., Stevanovic, K., Berres, M.-L., Hashimoto, D., Mortha, A., Leboeuf, M., Li, X.-M., Mucida, D., et al. (2014). Crosstalk between muscularis macrophages and enteric neurons regulates gastrointestinal motility. *Cell* 158, 300–313.
- Avetisyan, M., Rood, J.E., Huerta Lopez, S., Sengupta, R., Wright-Jin, E., Dougherty, J.D., Behrens, E.M., and Heuckeroth, R.O. (2018). Muscularis macrophage development in the absence of an enteric nervous system. *Proc. Natl. Acad. Sci.* 115, 4696–4701.
- Rae, F., Woods, K., Sasmono, T., Campanale, N., Taylor, D., Ovchinnikov, D.A., Grimmond, S.M., Hume, D.A., Ricardo, S.D., and Little, M.H. (2007). Characterisation and trophic functions of murine embryonic macrophages based upon the use of a Csf1r-EGFP transgene reporter. *Dev. Biol.* 308, 232–246.
- Banaei-Bouchareb, L., Gouon-Evans, V., Samara-Boustani, D., Castellotti, M.C., Czernichow, P., Pollard, J.W., and Polak, M. (2004). Insulin cell mass is altered in Csf1op/Csf1op macrophage-deficient mice. *J. Leukoc. Biol.* 76, 359–367.
- Leid, J., Carrelha, J., Boukarabila, H., Epelman, S., Jacobsen, S.E.W., and Lavine, K.J. (2016). Primitive Embryonic Macrophages are Required for Coronary Development and Maturation. *Circ. Res.* 118, 1498–1511.
- Cahill, T.J., Sun, X., Ravaut, C., Villa del Campo, C., Klaurakis, K., Lupu, I.-E., Lord, A.M., Browne, C., Jacobsen, S.E.W., Greaves, D.R., et al. (2021). Tissue-resident macrophages regulate lymphatic vessel growth and patterning in the developing heart. *Development* 148, dev194563.
- Van Nguyen, A., and Pollard, J.W. (2002). Colony Stimulating Factor-1 Is Required to Recruit Macrophages into the Mammary Gland to Facilitate Mammary Ductal Outgrowth. *Dev. Biol.* 247, 11–25.
- Dawson, C.A., Pal, B., Vaillant, F., Gandolfo, L.C., Liu, Z., Blieriot, C., Ginhoux, F., Smyth, G.K., Lindeman, G.J., Mueller, S.N., et al. (2020). Tissue-resident ductal macrophages survey the mammary epithelium and facilitate tissue remodelling. *Nat. Cell Biol.* 22, 546–558.
- Erblich, B., Zhu, L., Etgen, A.M., Dobrenis, K., and Pollard, J.W. (2011). Absence of Colony Stimulation Factor-1 Receptor Results in Loss of Microglia, Disrupted Brain Development and Olfactory Deficits. *PLoS One* 6, e26317.
- Paolicelli, R.C., Bolasco, G., Pagani, F., Maggi, L., Scianni, M., Panzanelli, P., Giustetto, M., Ferreira, T.A., Guiducci, E., Dumas, L., et al. (2011). Synaptic pruning by microglia is necessary for normal brain development. *Science* (80–333), 1456–1458.
- Zhang, Y., Yu, G., Chu, H., Wang, X., Xiong, L., Cai, G., Liu, R., Gao, H., Tao, B., Li, W., et al. (2018). Macrophage-Associated PGK1 Phosphorylation Promotes Aerobic Glycolysis and Tumorigenesis. *Mol. Cell* 71, 201–215.e7.
- Odegaard, J.I., Ricardo-Gonzalez, R.R., Goforth, M.H., Morel, C.R., Subramanian, V., Mukundan, L., Red Eagle, A., Vats, D., Brombacher, F., Ferrante, A.W., et al. (2007). Macrophage-specific PPARgamma controls alternative activation and improves insulin resistance. *Nature* 447, 1116–1120.
- Nguyen, K.D., Qiu, Y., Cui, X., Goh, Y.P.S., Mwangi, J., David, T., Mukundan, L., Brombacher, F., Locksley, R.M., and Chawla, A. (2011). Alternatively activated macrophages produce catecholamines to sustain adaptive thermogenesis. *Nature* 480, 104–108.
- Hua, L., Shi, J., Shultz, L.D., and Ren, G. (2018). Genetic Models of Macrophage Depletion. In *Methods in Molecular Biology* (Humana Press Inc.), pp. 243–258.
- Spence, J.R., Mayhew, C.N., Rankin, S.A., Kuhar, M.F., Vallance, J.E., Tolle, K., Hoskins, E.E., Kalinichenko, V.V., Wells, S.I., Zorn, A.M., et al. (2011). Directed differentiation of human pluripotent stem cells into intestinal tissue in vitro. *Nature* 470, 105–109.
- McCracken, K.W., Howell, J.C., Wells, J.M., and Spence, J.R. (2011). Generating human intestinal tissue from pluripotent stem cells in vitro. *Nat. Protoc.* 6, 1920–1928.
- Wilgenburg, B. van, Browne, C., Vowles, J., and Cowley, S.A. (2013). Efficient, Long Term Production of Monocyte-Derived Macrophages from Human Pluripotent Stem Cells under Partly-Defined and Fully-Defined Conditions. *PLoS One* 8, e71098.
- Buchrieser, J., James, W., and Moore, M.D. (2017). Human Induced Pluripotent Stem Cell-Derived Macrophages Share Ontogeny with MYB-Independent Tissue-Resident Macrophages. *Stem Cell Rep.* 8, 334–345.
- Stremmel, C., Schuchert, R., Wagner, F., Thaler, R., Weinberger, T., Pick, R., Mass, E., Ishikawa-Ankerhold, H.C., Margraf, A., Hutter, S., et al. (2018). Yolk sac macrophage progenitors traffic to the embryo during defined stages of development. *Nat. Commun.* 9, 75.
- Kaufmann, M. (1994). *The Atlas of Mouse Development Revised* (Elsevier Ltd).
- Holloway, E.M., Czerwinski, M., Tsai, Y.-H., Wu, J.H., Wu, A., Childs, C.J., Walton, K.D., Sweet, C.W., Yu, Q., Glass, I., et al. (2021). Mapping Development of the Human Intestinal Niche at Single-Cell Resolution. *Cell Stem Cell* 28, 568–580.e4.
- Workman, M.J., Mahe, M.M., Trisno, S., Poling, H.M., Watson, C.L., Sundaram, N., Chang, C.-F., Schiesser, J., Aubert, P., Stanley, E.G., et al. (2016). Engineered human pluripotent-stem-cell-derived intestinal tissues with a functional enteric nervous system. *Nat. Med.* 23, 49–59.
- Watson, C.L., Mahe, M.M., Múnera, J., Howell, J.C., Sundaram, N., Poling, H.M., Schweitzer, J.I., Vallance, J.E., Mayhew, C.N., Sun, Y., et al. (2014). An in vivo model of human small intestine using pluripotent stem cells. *Nat. Med.* 20, 1310–1314.
- Holloway, E.M., Wu, J.H., Czerwinski, M., Sweet, C.W., Wu, A., Tsai, Y.H., Huang, S., Stoddard, A.E., Capeling, M.M., Glass, I., et al. (2020). Differentiation of Human Intestinal Organoids with Endogenous Vascular Endothelial Cells. *Dev. Cell* 54, 516–528.e7.
- Menke, J., Rabacal, W.A., Byrne, K.T., Iwata, Y., Schwartz, M.M., Stanley, E.R., Schwarting, A., and Kelley, V.R. (2009). Circulating CSF-1 Promotes

- Monocyte and Macrophage Phenotypes that Enhance Lupus Nephritis. *J. Am. Soc. Nephrol.* 20, 2581–2592.
34. Jones, C.V., and Ricardo, S.D. (2013). Macrophages and CSF-1. *Organogenesis* 9, 249–260.
 35. Mass, E., Ballesteros, I., Farlik, M., Halbritter, F., Günther, P., Crozet, L., Jacome-Galarza, C.E., Händler, K., Klughammer, J., Kobayashi, Y., et al. (2016). Specification of tissue-resident macrophages during organogenesis. *Science* 353, aaf4238.
 36. Rojo, R., Raper, A., Ozdemir, D.D., Lefevre, L., Grabert, K., Wollscheid-Lengeling, E., Bradford, B., Caruso, M., Gazova, I., Sánchez, A., et al. (2019). Deletion of a *Csf1r* enhancer selectively impacts CSF1R expression and development of tissue macrophage populations. *Nat. Commun.* 10, 3215.
 37. Keshvari, S., Caruso, M., Teakle, N., Batoon, L., Sehgal, A., Patkar, O.L., Ferrari-Cestari, M., Snell, C.E., Chen, C., Stevenson, A., et al. (2021). CSF1R-dependent macrophages control postnatal somatic growth and organ maturation. *PLoS Genet.* 17, e1009605.
 38. Wynn, T.A., and Vannella, K.M. (2016). Macrophages in Tissue Repair, Regeneration, and Fibrosis. *Immunity* 44, 450–462.
 39. Hopkinson-Woolley, J., Hughes, D., Gordon, S., and Martin, P. (1994). Macrophage recruitment during limb development and wound healing in the embryonic and foetal mouse. *J. Cell Sci.* 107, 1159–1167.
 40. Saha, S., Aranda, E., Hayakawa, Y., Bhanja, P., Atay, S., Brodin, N.P., Li, J., Asfaha, S., Liu, L., Tailor, Y., et al. (2016). Macrophage-derived extracellular vesicle-packaged WNTs rescue intestinal stem cells and enhance survival after radiation injury. *Nat. Commun.* 7, 13096.
 41. Beck, F., Erler, T., Russell, A., and James, R. (1995). Expression of *Cdx-2* in the mouse embryo and placenta: Possible role in patterning of the extra-embryonic membranes. *Dev. Dyn.* 204, 219–227.
 42. Serreze, D.V., Gaedeke, J.W., and Leiter, E.H. (1993). Hematopoietic stem-cell defects underlying abnormal macrophage development and maturation in NOD/Lt mice: defective regulation of cytokine receptors and protein kinase C. *Proc. Natl. Acad. Sci.* 90, 9625–9629.
 43. Serreze, D.V., Gaskins, H.R., and Leiter, E.H. (1993). Defects in the differentiation and function of antigen presenting cells in NOD/Lt mice. *J. Immunol.* 150, 2534–2543.
 44. Shultz, L.D., Schweitzer, P.A., Christianson, S.W., Gott, B., Schweitzer, I.B., Tennent, B., McKenna, S., Mobraaten, L., Rajan, T.V., and Greiner, D.L. (1995). Multiple defects in innate and adaptive immunologic function in NOD/LtSz-scid mice. *J. Immunol.* 154, 180–191.
 45. Shibata, S., Asano, T., Noguchi, A., Naito, M., Ogura, A., and Doi, K. (1998). Peritoneal macrophages play an important role in eliminating human cells from severe combined immunodeficient mice transplanted with human peripheral blood lymphocytes. *Immunology* 93, 524–532.
 46. Hu, Z., Van Rooijen, N., and Yang, Y.-G. (2011). Macrophages prevent human red blood cell reconstitution in immunodeficient mice. *Blood* 118, 5938–5946.
 47. Bain, C.C., Bravo-Blas, A., Scott, C.L., Perdiguer, E.G., Geissmann, F., Henri, S., Malissen, B., Osborne, L.C., Artis, D., and Mowat, A.M. (2014). Constant replenishment from circulating monocytes maintains the macrophage pool in the intestine of adult mice. *Nat. Immunol.* 15, 929–937.
 48. Takata, K., Kozaki, T., Lee, C.Z.W., Thion, M.S., Otsuka, M., Lim, S., Utami, K.H., Fidan, K., Park, D.S., Malleret, B., et al. (2017). Induced-Pluripotent-Stem-Cell-Derived Primitive Macrophages Provide a Platform for Modeling Tissue-Resident Macrophage Differentiation and Function. *Immunity* 47, 183–198.e6.
 49. Miller, A.J., Yu, Q., Czerwinski, M., Tsai, Y.-H., Conway, R.F., Wu, A., Holmway, E.M., Walker, T., Glass, I.A., Treutlein, B., et al. (2020). In Vitro and In Vivo Development of the Human Airway at Single-Cell Resolution. *Dev. Cell* 53, 117–128.e6.
 50. Triantafilou, K., Triantafilou, M., and Dedrick, R.L. (2001). A CD14-independent LPS receptor cluster. *Nat. Immunol.* 2, 338–345.
 51. Binder, R.J., and Srivastava, P.K. (2005). Peptides chaperoned by heat-shock proteins are a necessary and sufficient source of antigen in the cross-priming of CD8+ T cells. *Nat. Immunol.* 6, 593–599.
 52. Srivastava, P. (2002). Roles of heat-shock proteins in innate and adaptive immunity. *Nat. Rev. Immunol.* 2, 185–194.
 53. Cai, Y., Winn, M.E., Zehmer, J.K., Gillette, W.K., Lubkowski, J.T., Pilon, A.L., and Kimura, S. (2014). Preclinical evaluation of human secretoglobin 3A2 in mouse models of lung development and fibrosis. *Am. J. Physiol. Cell. Mol. Physiol.* 306, L10–L22.
 54. Dirami, G., Massaro, G.D., Clerch, L.B., Ryan, U.S., Reczek, P.R., and Massaro, D. (2004). Lung retinol storing cells synthesize and secrete retinoic acid, an inducer of alveolus formation. *Am. J. Physiol. Cell. Mol. Physiol.* 286, L249–L256.
 55. Krasny, L., Bland, P., Kogata, N., Wai, P., Howard, B.A., Natrajan, R.C., and Huang, P.H. (2018). SWATH mass spectrometry as a tool for quantitative profiling of the matrisome. *J. Proteomics* 189, 11–22.
 56. Brock, S.E., Rendon, B.E., Yaddanapudi, K., and Mitchell, R.A. (2012). Negative Regulation of AMP-activated Protein Kinase (AMPK) Activity by Macrophage Migration Inhibitory Factor (MIF) Family Members in Non-small Cell Lung Carcinomas. *J. Biol. Chem.* 287, 37917–37925.
 57. Miller, E.J., Li, J., Leng, L., McDonald, C., Atsumi, T., Bucala, R., and Young, L.H. (2008). Macrophage migration inhibitory factor stimulates AMP-activated protein kinase in the ischaemic heart. *Nature* 451, 578–582.
 58. Maaser, C., Eckmann, L., Paesold, G., Kim, H.S., and Kagnoff, M.F. (2002). Ubiquitous production of macrophage migration inhibitory factor by human gastric and intestinal epithelium. *Gastroenterology* 122, 667–680.
 59. Efremova, M., Vento-Tormo, M., Teichmann, S.A., and Vento-Tormo, R. (2020). CellPhoneDB: inferring cell-cell communication from combined expression of multi-subunit ligand-receptor complexes. *Nat. Protoc.* 15, 1484–1506.
 60. Komori, T., Tanaka, M., Senba, E., Miyajima, A., and Morikawa, Y. (2014). Deficiency of oncostatin M receptor β (OSMR β) exacerbates high-fat diet-induced obesity and related metabolic disorders in mice. *J. Biol. Chem.* 289, 13821–13837.
 61. Piquer-Garcia, I., Campderros, L., Taxerås, S.D., Gavalda-Navarro, A., Pardo, R., Vila, M., Pellitero, S., Martínez, E., Tarascó, J., Moreno, P., et al. (2020). A Role for Oncostatin M in the Impairment of Glucose Homeostasis in Obesity. *J. Clin. Endocrinol. Metab.* 105, e337–e348.
 62. Elks, C.M., Zha, P., Grant, R.W., Hang, H., Bailey, J.L., Burk, D.H., McNulty, M.A., Mynatt, R.L., and Stephens, J.M. (2016). Loss of Oncostatin M Signaling in Adipocytes Induces Insulin Resistance and Adipose Tissue Inflammation in Vivo. *J. Biol. Chem.* 291, 17066–17076.
 63. Komori, T., Tanaka, M., Senba, E., Miyajima, A., and Morikawa, Y. (2013). Lack of oncostatin M receptor β leads to adipose tissue inflammation and insulin resistance by switching macrophage phenotype. *J. Biol. Chem.* 288, 21861–21875.
 64. Tsuruta, S., Kawasaki, T., Machida, M., Iwatsuki, K., Inaba, A., Shibata, S., Shindo, T., Nakabayashi, K., Hakamada, K., Umezawa, A., et al. (2022). Development of Human Gut Organoids With Resident Tissue Macrophages as a Model of Intestinal Immune Responses. *Cell. Mol. Gastroenterol. Hepatol.* 14, 726–729.e5.
 65. Godwin, J.W., Pinto, A.R., and Rosenthal, N.A. (2013). Macrophages are required for adult salamander limb regeneration. *Proc. Natl. Acad. Sci.* 110, 9415–9420.
 66. Cao, J., O'Day, D.R., Pliner, H.A., Kingsley, P.D., Deng, M., Daza, R.M., Zager, M.A., Aldinger, K.A., Blecher-Gonen, R., Zhang, F., et al. (2020). A human cell atlas of fetal gene expression. *Science* 80, 370.
 67. Titilii-Torres, K.F., and Morris, A.C. (2022). Embryonic hyperglycemia perturbs the development of specific retinal cell types, including photoreceptors. *J. Cell Sci.* 135, jcs259187.
 68. Yin, M., Zhang, Y., Yu, H., and Li, X. (2021). Role of Hyperglycemia in the Senescence of Mesenchymal Stem Cells. *Front. Cell Dev. Biol.* 9, 665412.

69. Scott-Drechsel, D.E., Rugonyi, S., Marks, D.L., Thornburg, K.L., and Hinds, M.T. (2013). Hyperglycemia Slows Embryonic Growth and Suppresses Cell Cycle via Cyclin D1 and p21. *Diabetes* 62, 234.
70. Fraser, R.B., Waite, S.L., Wood, K.A., and Martin, K.L. (2007). Impact of hyperglycemia on early embryo development and embryopathy: in vitro experiments using a mouse model. *Hum. Reprod.* 22, 3059–3068.
71. Chen, D., Sun, Y., Wei, Y., Zhang, P., Rezaeian, A.H., Teruya-Feldstein, J., Gupta, S., Liang, H., Lin, H.-K., Hung, M.-C., et al. (2012). LIFR is a breast cancer metastasis suppressor upstream of the Hippo-YAP pathway and a prognostic marker. *Nat. Med.* 18, 1511–1517.
72. Carroll, T.D., Newton, I.P., Chen, Y., Blow, J.J., and Näthke, I. (2018). Lgr5+ intestinal stem cells reside in an unlicensed G1 phase. *J. Cell Biol.* 217, 1667–1685.
73. Miller, I., Min, M., Yang, C., Tian, C., Gookin, S., Carter, D., and Spencer, S.L. (2018). Ki67 is a Graded Rather than a Binary Marker of Proliferation versus Quiescence. *Cell Rep.* 24, 1105.
74. Sauter, K.A., Pridans, C., Sehgal, A., Tsai, Y.T., Bradford, B.M., Raza, S., Moffat, L., Gow, D.J., Beard, P.M., Mabbott, N.A., et al. (2014). Pleiotropic effects of extended blockade of CSF1R signaling in adult mice. *J. Leukoc. Biol.* 96, 265–274.
75. Kim, J.E., Li, B., Fei, L., Horne, R., Lee, D., Loe, A.K., Miyake, H., Ayar, E., Kim, D.K., Surette, M.G., et al. (2022). Gut microbiota promotes stem cell differentiation through macrophage and mesenchymal niches in early postnatal development. *Immunity* 55, 2300–2317.e6.
76. van de Laar, L., Saelens, W., De Prijck, S., Martens, L., Scott, C.L., Van Isterdael, G., Hoffmann, E., Beyaert, R., Saeys, Y., Lambrecht, B.N., et al. (2016). Yolk Sac Macrophages, Fetal Liver, and Adult Monocytes Can Colonize an Empty Niche and Develop into Functional Tissue-Resident Macrophages. *Immunity* 44, 755–768.
77. Hao, Y., Hao, S., Andersen-Nissen, E., Mauck, W.M., Zheng, S., Butler, A., Lee, M.J., Wilk, A.J., Darby, C., Zager, M., et al. (2021). Integrated analysis of multimodal single-cell data. *Cell* 184, 3573–3587.e29.
78. Schindelin, J., Arganda-Carreras, I., Frise, E., Kaynig, V., Longair, M., Pietzsch, T., Preibisch, S., Rueden, C., Saalfeld, S., Schmid, B., et al. (2012). Fiji: an open-source platform for biological-image analysis. *Nat. Methods* 9, 676–682.
79. Stirling, D. R., Swain-Bowden, M. J., Lucas, A. M., Carpenter, A. E., Cimini, B. A., and Goodman, A. (2021). CellProfiler 4: improvements in speed, utility and usability. *BMC Bioinform.* 22, 433.
80. Liu, D., Song, A.T., Qi, X., van Vliet, P.P., Xiao, J., Xiong, F., Andelfinger, G., and Nattel, S. (2021). Cohesin-protein Shugoshin-1 controls cardiac automaticity via HCN4 pacemaker channel. *Nat. Commun.* 12, 2551.
81. Roberts, B., Haupt, A., Tucker, A., Grancharova, T., Arakaki, J., Fuqua, M.A., Nelson, A., Hookway, C., Ludmann, S.A., Mueller, I.A., et al. (2017). Systematic gene tagging using CRISPR/Cas9 in human stem cells to illuminate cell organization. *Mol. Biol. Cell* 28, 2854–2874.
82. Múnera, J.O., Sundaram, N., Rankin, S.A., Hill, D., Watson, C., Mahe, M., Vallance, J.E., Shroyer, N.F., Sinagoga, K.L., Zarzoso-Lacoste, A., et al. (2017). Differentiation of Human Pluripotent Stem Cells into Colonic Organoids via Transient Activation of BMP Signaling. *Cell Stem Cell* 21, 51–64.e6.
83. Bajpai, R., Chen, D.A., Rada-Iglesias, A., Zhang, J., Xiong, Y., Helms, J., Chang, C.-P., Zhao, Y., Swigut, T., and Wysocka, J. (2010). CHD7 cooperates with PBAF to control multipotent neural crest formation. *Nature* 463, 958–962.
84. Díaz-Rodríguez, Y., Cordeiro, P., Belounis, A., Herblot, S., and Duval, M. (2017). In vitro differentiated plasmacytoid dendritic cells as a tool to induce anti-leukemia activity of natural killer cells. *Cancer Immunol. Immunother.* 66, 1307–1320.
85. Rink, I., Rink, J., Helmer, D., Sachs, D., and Schmitz, K. (2015). A Haptotaxis Assay for Leukocytes Based on Surface-Bound Chemokine Gradients. *J. Immunol.* 194, 5549–5558.
86. Young, M.D., and Behjati, S. (2020). SoupX removes ambient RNA contamination from droplet-based single-cell RNA sequencing data. *GigaScience* 9.
87. Wickham, H. (2016). ggplot2: Elegant Graphics for Data Analysis.
88. Zhou, Y., Zhou, B., Pache, L., Chang, M., Khodabakhshi, A.H., Tanaseichuk, O., Benner, C., and Chanda, S.K. (2019). Metascape provides a biologist-oriented resource for the analysis of systems-level datasets. *Nat. Commun.* 10, 1523.
89. Szklarczyk, D., Gable, A.L., Nastou, K.C., Lyon, D., Kirsch, R., Pyysalo, S., Doncheva, N.T., Legeay, M., Fang, T., Bork, P., et al. (2021). The STRING database in 2021: customizable protein–protein networks, and functional characterization of user-uploaded gene/measurement sets. *Nucleic Acids Res.* 49, D605–D612.
90. Subramanian, A., Tamayo, P., Mootha, V.K., Mukherjee, S., Ebert, B.L., Gillette, M.A., Paulovich, A., Pomeroy, S.L., Golub, T.R., Lander, E.S., et al. (2005). Gene set enrichment analysis: A knowledge-based approach for interpreting genome-wide expression profiles. *Proc. Natl. Acad. Sci. USA* 102, 15545–15550.

STAR★METHODS

KEY RESOURCES TABLE

REAGENT or RESOURCE	SOURCE	IDENTIFIER
Antibodies		
CDH1	R&D systems	AF648
AIF1	FujiFilmWako	019-19741
CD14	Biolegend	325602
GFP_rabbit	Invitrogen	G10362
GFP_goat	Abcam	ab6673
CDX2	Abcam	ab157524
MKI67	Thermofisher	14-5698-82
Cleaved Caspase 3 (CC3)	New England Biolabs	9664S
ELAVL4	Thermofisher	A21271
TUBB3	Abcam	ab18207
PHOX2B	R&D sysytems	AF4940
S100B	Biolegend	676603
SMTN	Abcam	ab204603
SOX17	R&D sysytems	AF1924
FOXA2	Abcam	ab108396
NES	Biolegend	656801
VIM	Biolegend	677802
CD34	BioLegend	343506
CD45	BioLegend	368512
CD14	BD Horizon	565283
CD206	BioLegend	321108
CD163	BD Horizon	563888
CD16	BioLegend	302046
CD11b	BioLegend	301348
HLADR	BD Pharmingen	555812
Alexa Fluor 555 anti-rabbit	Thermofisher	A31572
Alexa Fluor 488 anti-rabbit	Thermofisher	A21206
Alexa Fluor 647 anti-mouse	Thermofisher	A31571
Alexa Fluor 488 anti-goat	Thermofisher	A11078
Dylight 550 anti-rat	Thermofisher	SA5-10027
Biological samples		
Day119 fetal proximal intestine	This paper	N/A
Chemicals, peptides, and recombinant proteins		
ActivinA	Thermofisher	338ac010
FGF4	Thermofisher	235F4025CF
CHIR99021	Selleckchem	S1263 2mg
EGF	Peptotech	AF-100-15
Noggin	Thermofisher	6057NG025CF
Insulin	Sigma Aldrich	I2643-25MG
basic-FGF (FGF2)	Peptotech	100-18B
Retinoic acid	Sigma Aldrich	R2625

(Continued on next page)

Continued

REAGENT or RESOURCE	SOURCE	IDENTIFIER
SCF	Miltenyi	130-094-303
VEGF	Peptotech	100-20
BMP4	ThermoFisher	PHC9534
IL3	ThermoFisher	PHC0031
MCSF	ThermoFisher	PHC9501
Critical commercial assays		
Chromium Next GEM Single Cell 3' Kit v3.1, 16 rxns	10X Genomics	PN-1000268
Glycolytic stress test kit	Agilent technologies	103020-100
CD14 Microbeads	Miltenyi Biotec	130-050-201
FastStart Universal SYBR Green Master	Roche	4913914001
pHrodo Red E. coli BioParticles	ThermoFisher	P35361
Deposited data		
Single-cell RNAseq datasets	SRA	PRJNA890190
Experimental models: Cell lines		
SEC61BGFP	Allen Institute for Cell Science	AICS-0010
SJi3252C2	This paper	N/A
SJ3013C2	This paper	N/A
EU03.C2	This paper	N/A
EU148.C5	This paper	N/A
Experimental models: Organisms/strains		
NOD.Cg-Prkdc ^{scid} Il2rg ^{tm1Wjl} /SzJ (NSG) mus musculus	Jackson Laboratories	005557
Oligonucleotides		
See Data Table S1	This paper	N/A
Software and algorithms		
R studio	R studio	https://www.rstudio.com/
Seurat	Hao et al., 2021 ⁷⁷	https://satijalab.org/seurat/articles/install
CellphoneDB	Efremova et al., 2020 ⁵⁹	https://github.com/ventolab/CellphoneDB
ImageJ (Fiji)	Schindelin et al., 2012 ⁷⁸	https://imagej.net/software/fiji/
Graphpad Prism 7	Dotmatics	https://www.graphpad.com/scientific-software/prism/
AcqKnowledge 4.2 (isometric force)	BIOPAC	Contact manufacturer
CellProfiler	Stirling et al., 2021 ⁷⁹	https://cellprofiler.org/

RESOURCE AVAILABILITY

Lead contact

Further information and requests for resources and reagents should be directed to and will be fulfilled by the lead contact, Gregor Andelfinger (gregor.andelfinger.med@ssss.gouv.qc.ca).

Materials availability

This study did not generate new unique reagents.

Data and code availability

- Single-cell RNA-seq data have been deposited at SRA and are publicly available as of the date of publication. Accession number NCBI: PRJNA890190.
- This paper does not report original code. Refer to [STAR Methods](#) details for single-cell RNA-seq analyses pipeline.
- Any additional information in this paper, including the microscopy data, required to reanalyze the data reported here is available from the [lead contact](#) upon request.

EXPERIMENTAL MODEL AND SUBJECT DETAILS

Cell lines and tissues

The use of human pluripotent stem cells was approved by the ethical committee at the participating institution CHU-Sainte Justine, Montreal QC, Canada (CER#2287). The hiPSCs and their derivations were routinely tested for mycoplasma (LT07-118, Lonza) and tested negative. Informed consent was obtained from all donors from whom the hiPSCs were derived. Five hiPSC lines were used in this study. SJi3252C2 and SJ3013C2 were derived from human fibroblasts of 40-year-old European males. EU03.C2 and EU148.C5 were derived from human peripheral blood mononuclear cell (PBMC) of 30-year-old European males. AICS-0010 (hiPSC^{eGFP} here) was acquired from Allen Institute for Cell Science and derived from human fibroblast of 30-year-old Asian male.

Human fetal (day 119) tissue of a European male was obtained after written informed consent and was approved by the ethical committee of CHU Sainte-Justine, Montreal QC, Canada (CER#2126).

Mice

The animal procedures were approved by the animal committee of CHU Sainte-Justine, Montreal QC, Canada (CIBPAR#2021–3202, 2022–3784). Maintenance and care were carried out in accordance with local guidelines. For grafting experiments, 6- to 8-week-old male immunodeficient *non-obese diabetic/Prkdc^{SCID}/Il2rg^{null}* (NSG) mice were used. For histological analysis, C57BL/6J mice at the corresponding developmental stage were used and the sex were not determined.

Pluripotent stem cell culture

Human induced pluripotent stem cells (hiPSC) were generated at CR-CHUSJ Stem Cell core or in-house. The hiPSC lines SJi3252C2 and SJ3013C2 were derived from human fibroblasts using Cytotune 1.0 (Invitrogen) and were previously characterized.⁸⁰ EU03.C2, and EU148.C5 were derived from human PBMC with Cytotune 2.0 (A16517, Invitrogen). The hiPSC^{eGFP} line (SEC61BGFP/AICS-0010) was acquired from Allen Institute for Cell Science.⁸¹ The abbreviations used for the above iPSC lines in this report are as follows: C1 (SJi3252C2), C2 (SJ3013C2), C3 (EU03.C2), C4 (AICS-0010), and C5 (EU148.C5). The hiPSCs were cultured in hypoxic condition (5% CO₂, 5% O₂, 37°C incubator) until passage 15–20, otherwise all cells and derivatives were cultured in normoxic condition (5% CO₂, 37°C incubator). They were cultured with mTeSR1 (85850, StemCell Technologies) with 1X penicillin-streptomycin (450-201-EL, MultiCell) and hESC-qualified Matrigel (354277, Corning). Matrigel was coated onto Nunc Delta surface plates (14-832-11, Thermo Scientific) as per manufacturer recommendation. The cells were passaged as small clusters using 0.5mM ethylenediaminetetraacetic acid (EDTA) in phosphate buffered saline (PBS). The cells were cryopreserved with NutriFreezD10 (05-713-1E, Biological Industries) as per manufacturer recommendation.

METHOD DETAILS

Human intestinal organoid derivation

Human intestinal organoids (HIO) were derived with the hiPSC-lines SJi3252C2 or SJ3013C2 as previously described with minor modifications.^{24,30,82} Briefly, 85% confluent hiPSCs in a 6 well plate were passaged with EDTA and seeded 1/14–1/16 of a cell suspension per single well of 24 well plate. The cells were fed mTeSR1 daily for two days or until the confluency reached 80%. On the first day, the media was changed with endoderm differentiation media base (EDM-base): RPMI1640 (11875-093, Gibco), 1X pen-strep (15015067, Wisent), 1X non essential amino acid (11140050, Gibco) with 100 ng/ml Activin A (338AC010, R&D systems). On the second day, the cells were fed EDM-base supplemented with 100 ng/ml Activin A and 0.2% FBS (HyClone, Fisher Scientific). On the third day, the cells were fed the same as the second but with 2% FBS. At the end of the third day, the monolayer expressed definitive endoderm markers SOX17 and FOXA2 (Figure 7A). The fourth day, the confluent monolayer of cells were fed with mid-hindgut differentiation media (MHDM): EDM-base, 2% FBS, 500 ng/ml FGF4 (235F4025CF, R&D systems), 3μM CHIR99021 (S1263, Selleckchem). The cells were fed MHDM daily for a total of 4 days. At the end of mid-hindgut differentiation, the free-floating spheroids were collected and suspended in Matrigel (354234, Corning) supplemented with 1X B27 supplement (17504044, Gibco) and 100 ng/ml EGF (236EG200, R&D systems; AF-100-15, PeproTech). The Matrigel suspension were plated as a droplet with 15–20 spheroids per droplet on a plate (14-832-11 or 130184, Thermo Scientific) and polymerized at 37°C for 10 min. Note that some tissue culture plate types are not suitable for Matrigel droplet formation. The spheroids were fed intestinal basal media (IBM): Advanced DMEM-F12 (12634-010, Gibco), 1X B27 (17504044, Gibco), 1X Glutamax (35050061, Gibco), 1X pen-strep, 15mM HEPES (15630080, Gibco) supplemented with 100 ng/ml EGF and 100 ng/ml Noggin (6057NG025CF, R&D systems) for four days changing the medium every 48 h. They were then fed IBM supplemented with 100 ng/ml EGF (IBMe) every 48 h. Two weeks after the spheroid collection, the organoids were passaged by manually separating from each other with sterile syringe needle and re-embedding in the Matrigel droplet as before. From this point onward, the organoids were fed IBMe and passaged every two weeks until the experiment. The organoids were positive for intestine-specific epithelial marker CDX2 (Figure 7A).

Vagal neural crest derivation

Vagal neural crest cells (VNCC) were derived from the hiPSC-line SJ3013C2 as previously described with minor modifications.^{30,83} Briefly, In a 6 well plate, small colonies of hiPSC were seeded at low density (1/80 of a confluent well of 6 well plate) and grown for

5 days. On the first day of differentiation, the colonies were lifted with 500U/ml collagenase IV (17104019, Gibco) in mTeSR1 for up to 1 hour in the incubator or until the colonies detached completely with gentle taps to the plate. The colonies were washed with 2 mL of DMEM/F12 (319-075-CL, Wisent) three times. They were then suspended in neural induction media (NIM): 1:1 ratio of DMEM-F12 and Neurobasal media (21103049, Gibco), 0.5X B27, 0.5X N2, 5 µg/ml insulin (I2643, Sigma), 20 ng/ml basic-FGF (100-18B, PeproTech), 20 ng/ml EGF, and 1X pen-strep with 5 µM of Rock inhibitor Y27632 (S1049, Selleckchem) and transferred to non-tissue culture treated plate (08-772-51, Fisher scientific). The NIM was changed daily with decreasing Y27632 (Y27) concentration (Day 2: 2.5 µM Y27, Day 3 and beyond: no Y27), for additional 5 to 6 days until the neurospheres had clear round borders. The neurospheres were then fed NIM with 2 µM all-trans-retinoic acid (R2625, Sigma Aldrich) daily for two days. The neurospheres were transferred on to the fibronectin (PHE0023, Gibco) coated plate in NIM (w/o retinoic acid) and left undisturbed for 48 hours. Fibronectin coated plates were prepared by incubating plastic tissue culture plates with 15 µg/ml fibronectin in PBS without calcium or magnesium at 37°C overnight. Afterward, the NIM was changed daily until neural crest cells migrated and spread out onto the plate (6–10 days). Neurospheres were mechanically removed and the migrated neural crest cells were lifted as single cells with a 5 min incubation at 37°C with 1X TrypLE (A1217701, Gibco). Cells were washed by diluting with 9 mL of room temperature DMEM/F12 and centrifuging at 300G for 4 min. The supernatant was removed and cells were resuspended in DMEM/F12 for co-culture with HIO or resuspended in NIM and plated back onto fibronectin coated plate and maintained until the experiment. The cells were positive for known vagal fate neural crest cell markers and gene expression (Figures 7B and 7C).

Macrophage derivation

Macrophages were derived from EU03.C2 or EU148.C5 or AICS-0010 as previously described with modifications.²⁵ Briefly, embryoid bodies (EB) were formed as follows. The hiPSC were cultured to 85–90% confluency in a 6 well plate with mTeSR1 and Geltrex matrix (A1413301, Gibco) and divided into smaller segments by scratching the bottom of the well into around 100 squares with a 100 µl tip. The segments were detached mechanically with a scraper and the cells clumps were transferred into 6 well ultra-low attachment plate (3471, Corning) with EB media: mTeSR1 supplemented with 50 ng/mL BMP4 (120-05ET, PeproTech), 50 ng/mL of VEGF (100-20A, PeproTech), 20 ng/ml of SCF (130-093-991, Miltenyi Biotec) and 10 µM Y-27632 (72304, Stem Cell Technologies) and cultured in a 37°C, 5%CO₂ incubator. Every two days, half of the EB media was replaced with fresh EB media without Y-27632 for a total of 7 days. The EBs were then transferred to a 6 well tissue plate (10–15 EBs/well) in Factory EB (f-EB) media consisting of X-VIVO15 (BE04-418F, Lonza) supplemented with 100 ng/mL of MCSF (216-GMP-500, R&D), 25 ng/mL of IL-3 (PHC0031, Gibco), 1X Glutamax, 1X pen-strep and 0.055 mM β-mercaptoethanol (31350-010, Invitrogen). The f-EB media were replaced weekly. Macrophage precursors started to emerge in the supernatant after approximately 15–20 days, reaching the maturity after 30 to 45 days in f-EBs cultures, assessed by the cell surface markers expression (CD34^{neg or low}, CD14^{high}, CD45^{high}) through flow cytometry (Figure 7D). The precursors were harvested every two weeks for experimentation. Harvested precursors were cultured in RPMI media (SH3009601, Hyclone) supplemented with 100 ng/ml of MCSF, 2 mM L-glutamine, 10% FBS (080150, Wisent) and 1X pen-strep for 7 days, replacing the media every two days. Differentiated macrophages were assessed with flow cytometry for the expression of macrophage markers (CD14^{high}, CD206^{high}, CD163^{high}, CD16^{high}, CD11b^{high}, HLADR^{neg}) (Figures 7E and 7F). Additionally, dendritic cell marker FLT3 expression in the macrophages were low to none (Figures S2A and S2B).

HIO combination with VNCC and macrophage

Prior to the procedure, two to three week HIOs (since spheroid collection), differentiated macrophages, and vagal neural crest cells were derived as required. Matrigel was supplemented with 1X B27 and 100 ng/ml EGF. In a 5 mL tube, 50K VNCC and/or 100K macrophages were added to maximum x15 HIOs. Optimal number of VNCC and macrophages may vary depending on the cell line. The mix was briefly titrated using a 1000 µl pipette-tip, kept at –20°C, where 1 mm of the end of the tip was cut. The mix was then centrifuged at 300G for 3 min. The HIOs and the cells were then gently resuspended and centrifuged again. Supernatant was removed as much as possible and 50 µl of cold Matrigel was added. The tube was kept on a cold tube from this point on. Using a cut-pipette tip that is cold, HIO and cells were gently resuspended and the total volume was gently pipetted as a droplet on a pre-warmed 6 well plate. Up to four droplets were plated per well. The plate was gently transferred to the incubator and allowed to polymerize for 10 min. The well was then filled with 2 mL of IBMe supplemented with 20 ng/ml MCSF (Thermofisher, PHC9501; PeproTech, 300-25). After 48 hr, the medium was replaced with fresh IBMe. The medium was refreshed every 48 hr. One week after the co-culture, the organoids were removed from the Matrigel with gentle titration and dissection with sterile syringe needles. They were then re-embedded in new Matrigel droplets. HIOs were maintained with IBMe on the same feeding interval as before for another week before experimentation unless specified otherwise.

Human dendritic cell

Human dendritic cells used as positive control for FLT3 qPCR were derived from purified cord blood CD34⁺ progenitors as previously described.⁸⁴

Immunocytochemistry

Cells were grown on plastic coverslips (174969, Thermo Fisher). At room temperature, cells were washed once with PBS and fixed in 4% paraformaldehyde (PFA) for 10 min. PFA was removed and washed three times with cold PBS 5 min each. Cells were then

incubated in blocking buffer (0.5% Triton X-100 and 10% donkey serum in PBS) for 1 hr. Blocking buffer was removed and cells were incubated with primary antibody in blocking buffer at 4°C overnight. The next day, primary antibody buffer was removed and cells were washed in cold PBS four times 4 minutes each then incubated in secondary antibody in blocking buffer for 1 hour at room temperature in the dark. The secondary antibody buffer was removed and cells were washed in PBS four times 4 minutes each. Cells were then stained with DAPI (D-21490, Invitrogen) and washed once with distilled water. The coverslip was mounted on a 1.5 coverslips with aqueous mounting medium (S3023, Dako) as per manufacturer recommendation before imaging.

Immunofluorescence and histology

In vitro organoids, E9.5, and E10.5 mouse embryos were fixed with 4% PFA for 3 hours at 4°C. Fetal proximal intestine, grafted organoids (cut in half), E12.5, and E15.5 mouse embryos (heads removed) were fixed for 12–16 h at 4°C. The samples were washed with PBS on ice for 1 hour three times with rocking and incubated in 30% sucrose in PBS at 4°C until it sank. It was then incubated with optimal cutting temperature (OCT, FSC22, Surgipath) compound at 4°C for 30 min, frozen-embedded in fresh OCT, and stored at –80°C. The samples were cut 5–10 µm thickness and mounted on a charged glass slide (12-550-15, Fisherbrand). The sections were dried at room temperature for minimum 30 minutes before the staining procedure. The sections were washed with PBS for 5 min two times and incubated in 0.5% Triton X-100 in PBS for 20 min. They were then incubated in the blocking buffer (10% Donkey serum and 0.3% Triton X-100 in PBS) for 30 min and incubated with primary antibody overnight at 4°C in a humid chamber. The next day, the slides were washed three times for 5 min each in PBS and incubated with the secondary antibody buffer for 1 hour at room temperature. The slides were washed four times for 5 min each in PBS. The sections were counterstained with DAPI (D-21490, Invitrogen) for 10 min and washed once with distilled water. The slides were mounted with aqueous mounting medium (S3023, DAKO) with 1.5 glass coverslip and cured overnight at room temperature. The samples were then imaged with widefield (DMI8, Leica) or confocal (TCS SP8, Leica) microscope. Colorimetric staining (H&E + S and TMS) were performed by CHU-Sainte Justine pathology laboratory.

Quantitative PCR

RNA was isolated with a DNase treatment (74104, 79254, Qiagen; Z6111, Promega) and cDNA was synthesized (18090050, Invitrogen) with oligo-dT (18418012, Invitrogen). SyberGreen (34226600, Roche) was used to quantify gene expression with Roche LightCycler 96 or LightCycler 480. A total of 15 ng of cDNA and 0.3 µM of each primer pair was used for a 15 µl reaction as per manufacturer instruction. The primer sequences were designed using NCBI Primer-BLAST. Refer to [Table S1](#) for the list of primer sequences.

Grafting of organoids to immunodeficient mice

Two to three weeks after the macrophage co-culture, organoids with single epithelial structure were grafted under the kidney capsules of immunodeficient mice as previously described, but without the collagen encapsulation of the organoid prior to grafting.³¹ The organoids were collected at corresponding time points.

E.Coli particles injection into the grafted organoid lumen

Kidneys with the grafted HIO/Macs were surgically exposed again 10 weeks after the engraftment. With an insulin syringe, up to 50–200 µl of fluid was removed from the lumen of the organoid and an equal volume of 4 mg/ml of pH-sensitive E.Coli Bioparticle (P35361, Thermofisher) reconstituted in PBS was injected into the lumen. The grafted kidney was placed back in the mice with the same procedure for grafting the organoids. The organoids were collected 24 h later, sectioned in half with a surgical scalpel, and fixed in 4% PFA for 3 h. The tissue was processed and examined with the method as described in ‘Immunofluorescence’ but stained only with DAPI.

Live imaging of injured HIO/Mac

HIO/Mac combined with hiPSC^{eGFP}-derived macrophages were cultured in suspension in ultra low attachment plate (3471, Corning) with phenol-free IBMe for two days prior to injury. Advanced DMEM-F12 was replaced with high-glucose phenol-free DMEMF12 (D1145, SigmaAldrich) to make phenol-free IBMe. To injure the organoid, 20G blunt tip needle attached to a 1 mL syringe was used to puncture the organoid at the center. The plunger was drawn slowly as pulling back to remove the punctured material. The injured organoid was then placed in a glass-bottom dish (0030 740.017, Eppendorf) with phenol-free IBMe and imaged at a 10 min interval for 12–18 hours with up to a 100 µm z-depth (TCS SP8 confocal or DMI8 widefield, Leica). The stage-top incubator was set at 5% CO₂ at 37°C (iNU GSI2, Tokaihit). From the maximal projection image, cells were tracked with ImageJ plugin: Manual Tracking. The region of the injury was determined *in situ* from the images and the center of that region was used for downstream analysis. For controls, an arbitrary point at the center of the image was set, blinded from tracking of the cells. Directness and chemotactic precision index (CPI) were calculated as previously described.⁸⁵

Isometric force measurement

At week 12 of engraftment, HIO/ENS and HIO/ENS/Mac were isolated from the mice into Krebs buffer (NaCl 117 mM, KCl 4.7 mM, MgCl hexahydrate 1.2 mM, NaH₂PO₄ 1.2 mM, NaHCO₃ 25 mM, CaCl₂ dihydrate 2.5 mM, Glucose 11 mM). Each whole organoid

was then hooked at the opposite end with silk strings and transferred to organ bath chambers with 37°C Krebs buffer fed with 95% O₂ and 5%CO₂. The samples were then connected to the isometric force transducer and equilibrated at 1g of tension for an hour before the acquisition (Biopac MP150; Acqknowledge, Biopac). Spontaneous contractions were measured for 20-40min. The last 20min segment of regular contractions were taken for analyses. Maximal force is the highest peak. Contraction and relaxation time are averages of measure from trough to peak and peak to trough, respectively. Frequency of contraction is the number of peaks.

Single cell RNA sequencing and analysis

For the preparation of single cell suspension, all samples were cut into <1 mm pieces using a scalpel and dissociated using 1000U/ml collagenase IV (17104019, Thermofisher) in 2X TrypLE (A1217701, Thermofisher) with 10mM Glucose for 100-120minutes at 37°C. The suspension was gently titrated every 10 min to facilitate the dissociation. Cells were then passed through a 70um filter and 10-fold diluted in cold 1%FBS in PBS. The cells were then centrifuged 500G 5 min at 4°C. The pellet was resuspended in 1%FBS in PBS and viable cell numbers were quantified with trypan blue and hemocytometer. For grafted day 121 HIO/ENS/Mac, GFP⁺ macrophages were enriched using fluorescence-activated cell sorting (FACS). The cDNA and the libraries were then generated using Chromium Next GEM v3.1 according to the manufacturer guideline (1000268, 10X Genomics; manual: CG000315 RevB) and sequenced at Génome Québec with Novaseq 6000 S4 (20027466, Illumina). Human fetal scRNAseq FASTQs were acquired from ArrayExpress: E-MTAB-8221, E-MTAB-9720.^{29,49} For the comparison of human fetal and organoid datasets, both were processed with SoupX to negate the effect of ambient RNA, largely arising from the red blood cells.⁸⁶ Otherwise, FASTQs were processed with CellRanger and downstream analyses performed with R using Seurat and visualized with ggplot2.^{77,87} When the sex of the samples could not be matched in differential gene expression, chromosome X and Y genes were omitted from further analyses and visualization. Gene ontology analyses were performed with Metascape and protein association analyses with STRING.^{88,89} Gene set enrichment analysis was performed with GSEA software.⁹⁰

Glycolytic stress test

Mesenchyme of HIOs co-cultured with or without macrophages for 7 days were dissected and dissociated into single cells with the same method as described in 'Single cell RNA sequencing and analysis'. In order to remove the macrophages from the cell suspension, all samples were processed with magnetic cell sorting with CD14 Microbead (130-050-200, Miltenyi biotec), LS column (130-042-401), and MidiMACS Separator (130-042-302) according to the manufacturer recommendation. Sorted cell suspension were centrifuged 400G for 5 min at 4°C. Cells were resuspended in 4°C IBM, counted using hemocytometer, and 50K cells per well in 180ul volume were distributed to the Seahorse 96well microplate (101085-004, Agilent) pre-coated with hESC-qualified Matrigel (354277, Corning) as per manufacturer instructions. The plate was then centrifuged 300G for 1min. The mesenchymal cells were incubated at 5%CO₂, 37°C incubator for 1 h for cell attachment. Subsequently, the culture media was replaced with 37°C assay media (DMEM 5030 media, 2mM glutamine) and equilibrated at 37°C non-CO₂ incubator for 1 h prior to extracellular acidification rate (ECAR) measurements with the Seahorse XFe96 Flux Analyzer. Following reagents were prepared according to the manufacturer instruction to perform the glycolytic stress test: 10mM Glucose, 5μM Oligomycin (O4876, Sigma-Aldrich), 100mM 2-Deoxy-D-glucose (2-DG, sc-202010A, Santa Cruz).

OSM treatment

Mesenchyme of HIOs were dissected and dissociated into single cells with the same method as described in ‘Single cell RNA sequencing and analysis’. Up to 80K cells were seeded on to Matrigel coated 6 well plate. See ‘Pluripotent stem cell culture’ for Matrigel coating. The cells were fed 2mL of fresh IBMe every 2 days until 50% confluency. The cell culture media was changed then changed to IBMe containing 500 ng/ml OSM or vehicle (0.1%BSA in PBS). The media was refreshed with the corresponding condition after 24 h. After 48 h total in experimental conditions, the cells were lysed directly from the plates using the lysis buffer of the RNA extraction kit (74104, 79254, Qiagen; Z6111, Promega) and proceeded to ‘Quantitative PCR’ procedure as described above.

QUANTIFICATION AND STATISTICAL ANALYSIS

The number of biologically independent samples (e.g., organoids) or animals is indicated by “n”, whereas each organoid single cell RNAseq dataset in this study is a pool of 4–5 dissociated organoids. “N.S.” means not significant. All relevant figures are in mean and error bars are in standard deviation (“s.d.”). In single cell transcriptomic comparison between fetal and organoid samples, the threshold of discovery (dotted line) were log2fold change >1, adjusted p value <0.001 where Wilcoxon rank-sum test was used. For comparison of organoid size between two conditions, two-dimensional area of the image of organoid was quantified with ImageJ and the weight of the organoid was measured by scale⁷⁸. Welch’s t test was used for statistical testing. For exponential regression of the size of the grafted organoids over time from two-way ANOVA was used. For quantification of level of apoptosis in grafted organoids, the area of cleaved caspase 3 divided by the area of nuclei (DAPI) in confocal microscopy images of immunofluorescence using imageJ and CellProfiler^{78,79}. Welch’s t test was used for statistical testing. For combined size comparison of all 10 week grafted organoids, one way ANOVA was used and posthoc Tukey. For quantification of epithelial length, epithelial length was measured from the tip of the epithelium (in lumen) to the closest tip of the crypt. Epithelial length was divided by the thickness of the tissue to calculate the ratio. The measurement was repeated three locales per sample to attain the mean. Student’s t-test was performed for statistics.

For single cell transcriptomic comparison between *in vitro* organoids with or without macrophages, threshold of discovery was set to adjusted p value <0.001 , Log2fold change >0.09 & <-0.09 where Wilcoxon rank-sum test was used. For statistical analysis of ECAR time course two-way ANOVA was used with post-hoc Sidak-Bonferroni. For glycolysis and glycolytic in the glycolytic stress test, following formula was used: Glycolysis (maximum rate measurement before oligomycin measurement – last rate measurement before glucose injection), glycolytic capacity (maximum rate measurement after oligomycin measurement - last rate measurement before glucose injection), and non-glycolytic acidification (last rate measurement prior to glucose injection). Student's t-test was used for statistics and each data point represent a technical replicate well. Specific statistical details for each experiment can be found in the figure legends.

Statistical analyses were performed using GraphPad Prism v.7.04 and R statistical software.

Supplemental information

**Developmental role of macrophages
modeled in human pluripotent stem
cell-derived intestinal tissue**

Andrew T. Song, Renata H.M. Sindeaux, Yuanyi Li, Hicham Affia, Tapan Agnihotri, Severine Leclerc, Patrick Piet van Vliet, Mathieu Colas, Jean-Victor Guimond, Natalie Patey, Lara Feulner, Jean-Sebastien Joyal, Elie Haddad, Luis Barreiro, and Gregor Andelfinger

Supplemental Text and Figures

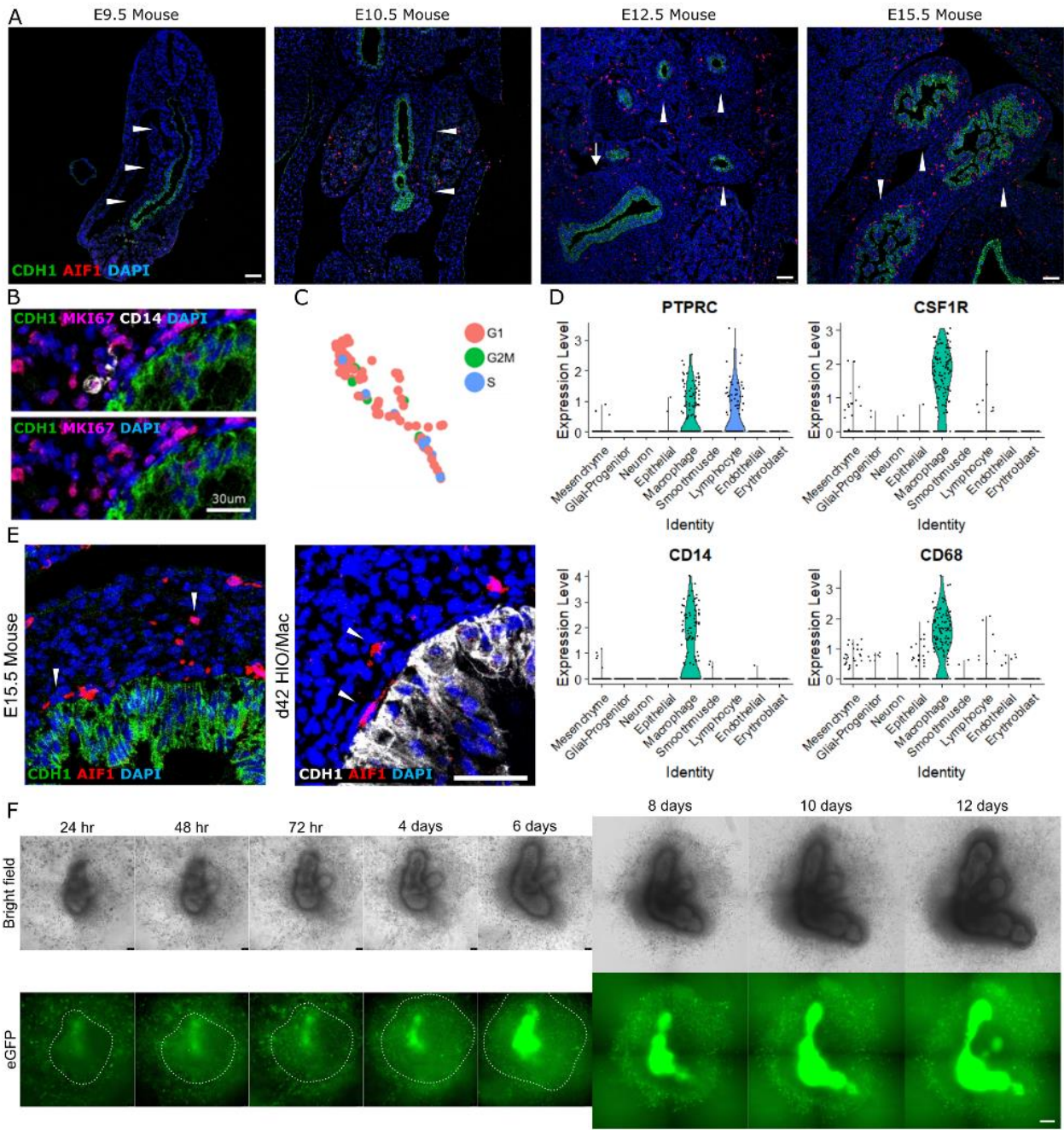


Figure S1. Macrophages in early embryonic mouse intestine, fetal intestine, and human intestinal organoid (HIO), related to Figure1 & 2 & 4.

- (A) Representative immunofluorescence images of mouse embryonic intestine for macrophages (AIF1), epithelium (CDH1), and nuclei (DAPI) at four time points of development. Arrowhead, mid-hindgut. Arrow, Foregut. E9.5, n=4, E10.5, n=6, E12.5, n=6, E15.5, n=6. Scale bar = 75µm.
- (B) Representative immunofluorescence image of day 42 HIO/Mac for epithelium (CDH1), proliferation (MKI67), macrophages (CD14), and nuclei (DAPI). Scale bar = 30µm.
- (C) Cell cycle status of macrophages in day 37 HIO/ENS/Mac (C1/C2/C5) from scRNAseq.
- (D) Violin plot of gene markers used to identify the unsupervised cluster as macrophage in scRNAseq.
- (E) Representative immunofluorescence images for macrophages (AIF1), epithelium (CDH1), and nuclei (DAPI) in E15.5 mouse intestine and day 42 HIO/Mac. Arrowhead, macrophages localized at adjacent to epithelium and within mesenchyme. Scale bar = 50µm.
- (F) Bright field and GFP fluorescence images of human intestinal organoid (HIO) and macrophage co-culture over the course of 12 days. Macrophages were derived from hiPSC^{eGFP}. Scale bar = 150µm.

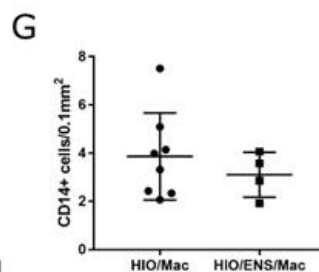
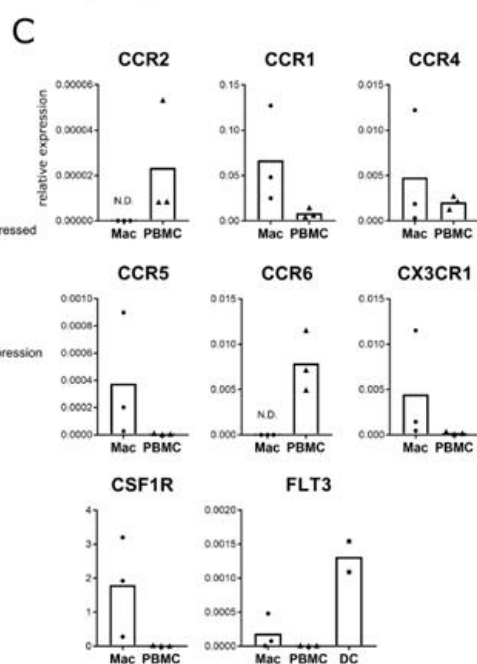
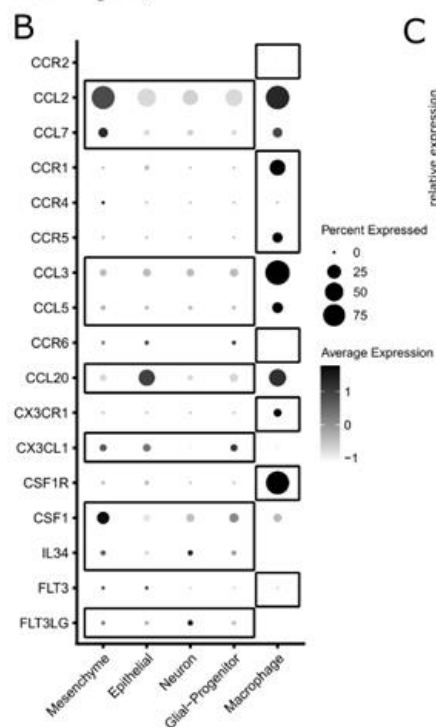
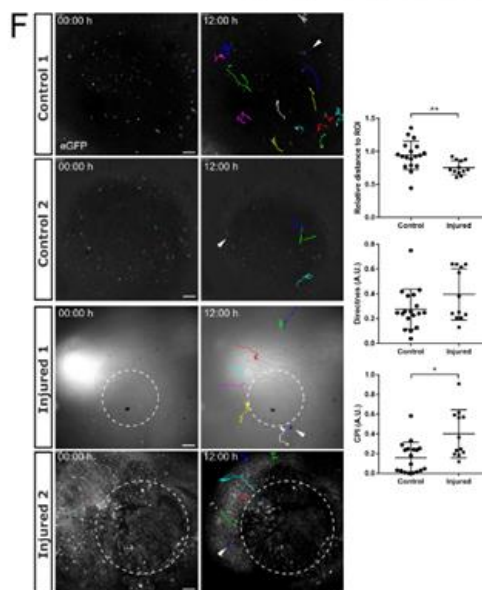
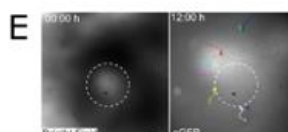
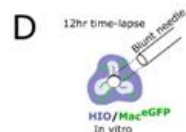
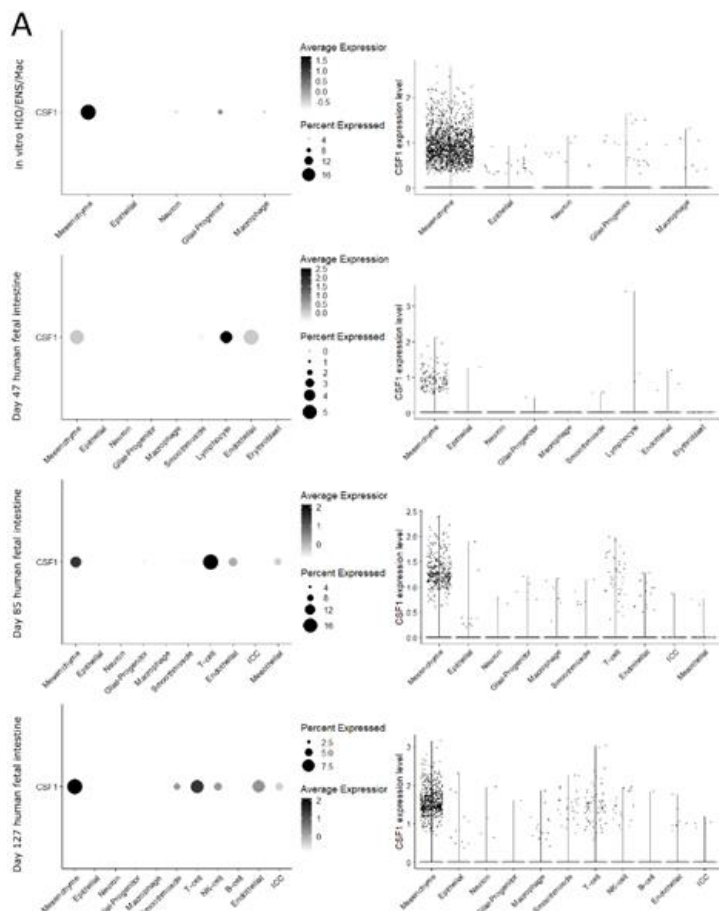


Figure S2. Migration and retention of macrophages in the organoid, related to Figure1 & 2.

- (A) Dot plots and violin plots of *CSF1* expression in presumptively annotated unsupervised clusters of the day 37 organoid, day 47, day 85, day 127 fetal intestine datasets. Dot plots: Percent Expressed, percentage of cells within the cluster expressing the gene. Violin plot: Each dot represents a cell.
- (B) Dot plot of ligand and receptor involved in macrophage recruitment in scRNAseq of HIO/ENS/Mac (C1/C2/C5).
- (C) qPCR of receptor genes for hiPSC-derived macrophages (Mac [C2, C3, C5]) prior to co-culture with HIO. Peripheral blood mononuclear cell (PBMC) and dendritic cell (DC) used as a reference previously shown to express the genes. Normalized to GAPDH expression. Mac, n = 3, PBMC, n = 3, DC, n = 2, biological replicates.
- (D) Schematic of the *in vitro* organoid puncture injury.
- (E) Demarcation of the injury as indicated by the bright field image and the corresponding hiPSC^{eGFP}-derived macrophages (Mac^{eGFP}) tracing.
- (F) Representative GFP fluorescence images from the 12-hour time lapses of control and injured *in vitro* HIO/Mac^{eGFP} (C1/C4). Colored lines and dots: tracing of the macrophage location over time. Dotted circle: region of the injury. Arrowhead: stationary points in the organoid to track the drifting of the entire sample. To the right: Quantification of relative distance of the macrophages, at 12 hour vs. 0 hour, from the center of the injury (Injured) or an arbitrary point within the image determined blinded (control). A measure of straightness of cell trajectories quantified as directness. Degree of directed migration towards a region of interest quantified as chemotactic precision index (CPI). See STAR Methods for calculation. Control, n = 2 organoids, n = 18 cells, Injury, n = 2 organoids, n = 12 cells, each data point represents a cell. Mean & s.d. (d-f). p = 0.0037, Welch's t-test (d). p = 0.2486 (e), p = 0.0116 (f), Wilcoxon rank sum test (Mann-Whitney). Scale bar=100µm.
- (G) Quantification of macrophage numbers within day 42 HIO co-cultured only with macrophage or with macrophage and vagal neural crest cells (ENS precursor). CD14-positive macrophages counted in non-epithelial region of the organoid (CDH1-negative & DAPI-positive) cryosections. Each data point represents an organoid. Result of two experiments. iPSC lines: HIO=C1, ENS precursor=C1, macrophage=C2. Related to Figure 2F. HIO/Mac: n = 8. HIO/ENS/Mac: n = 4. Mean & s.d. P = 0.4577, student's t-test.

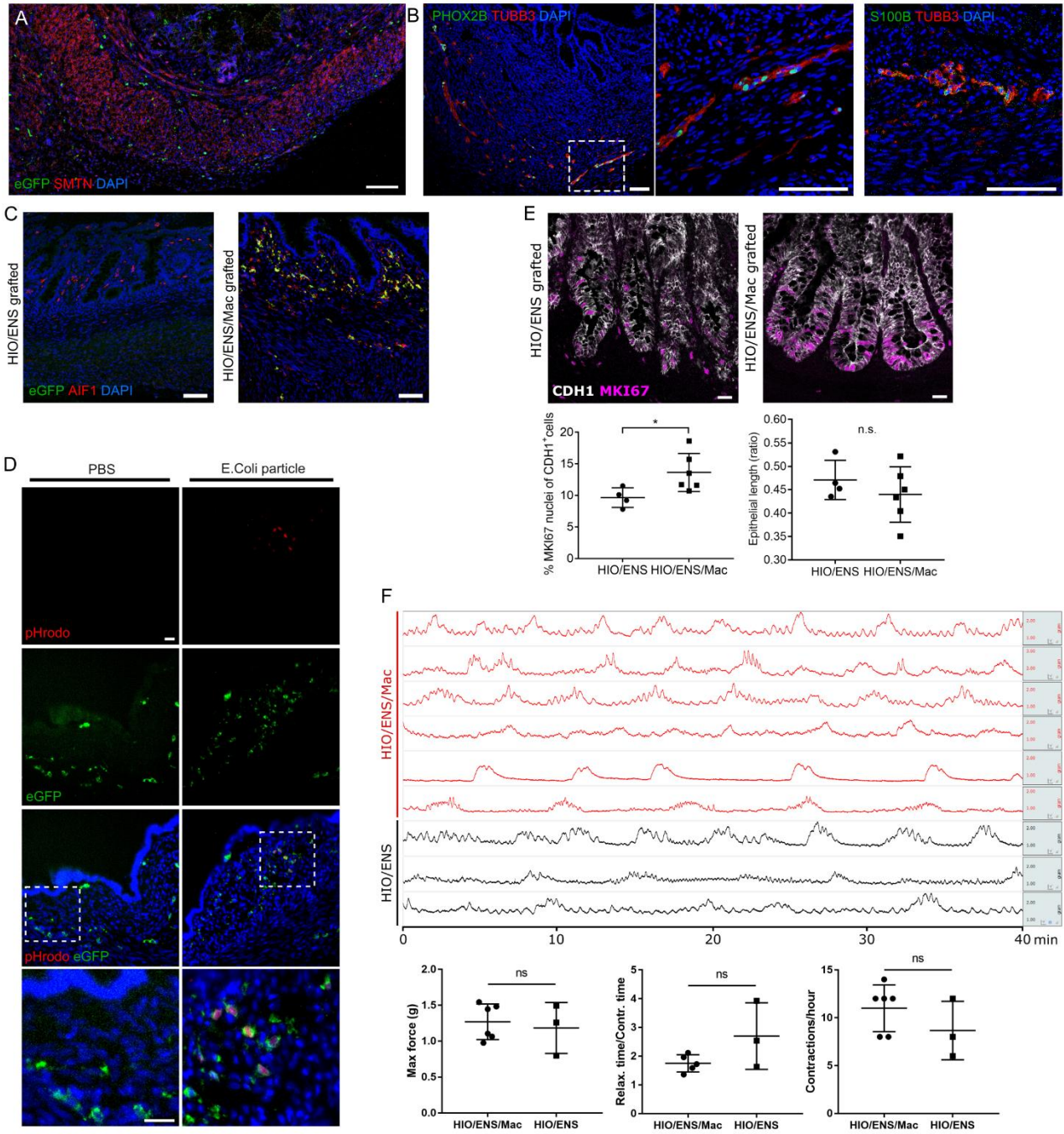
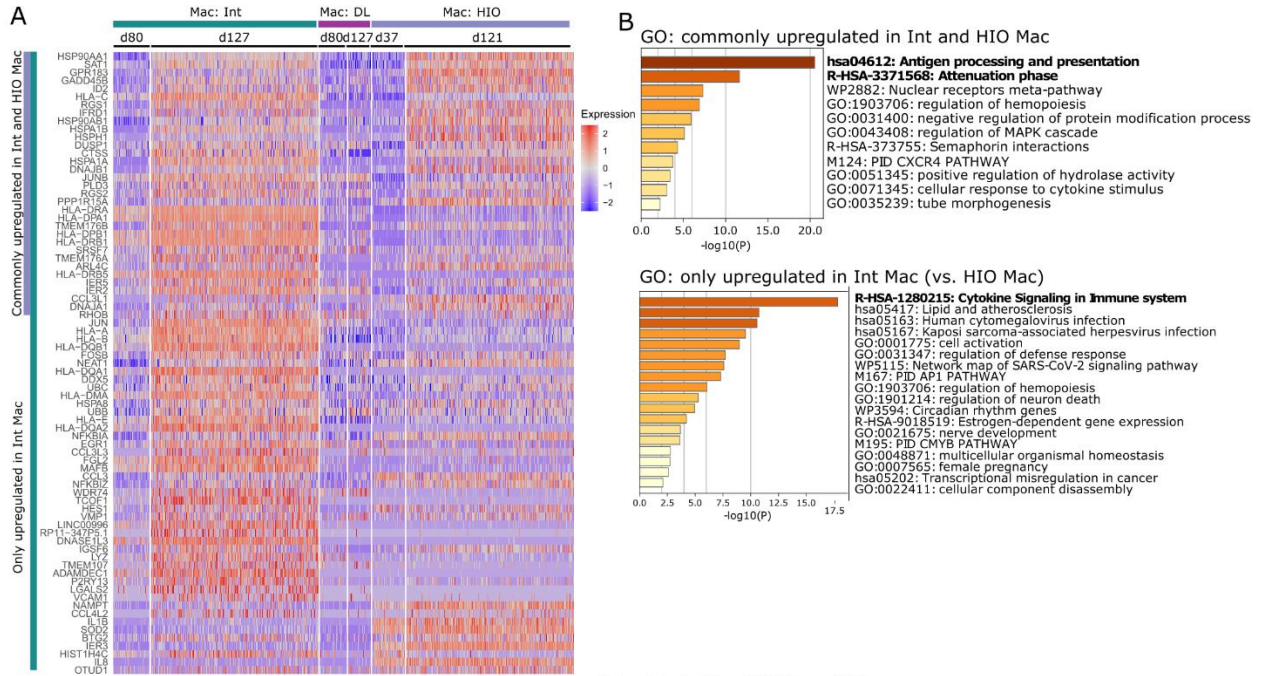
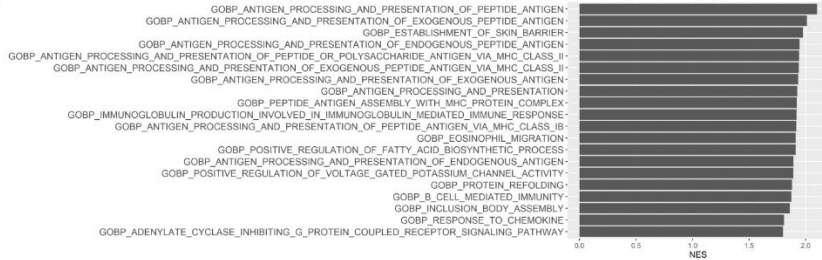


Figure S3. Characterization of grafted organoids, related to Figure 3.

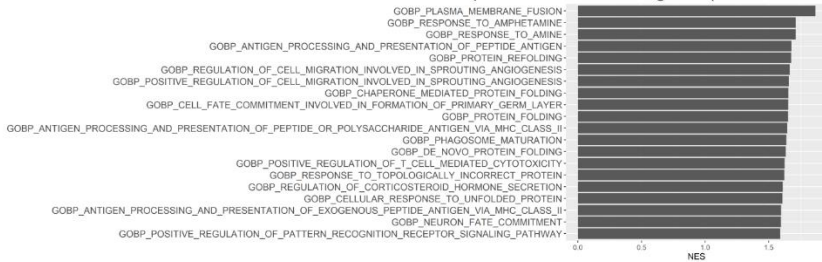
- (A) Representative immunofluorescence image of 10 week grafted HIO/ENS/Mac^{eGFP} probed for macrophages (eGFP), smooth muscle (SMTN). Nuclei (DAPI). Scale bar=100μm.
- (B) Representative immunofluorescence image of enteric neurons (PHOX2B, TUBB3) and glial cells (S100B) in 10 week grafted HIO/ENS/Mac. Nuclei (DAPI). Scale bar=100μm.
- (C) Representative immunofluorescence images of grafted organoids combined without (HIO/ENS) or with hiPSC^{eGFP} derived macrophages (HIO/ENS/Mac^{eGFP}). Probed for iPSC-derived macrophages (eGFP) and macrophages (AIF1). Scale bar=50μm.
- (D) Tissue sections of grafted HIO/Mac^{eGFP} (C1/C4) injected with pHrodo-E.Coli particle conjugates or PBS (vehicle) into the lumen. Tissue sections counterstained with DAPI. Internalized E.Coli signals were only found in flat epithelial areas. PBS control: n=3. pHrodo-E.Coli particle: n=2. Scale bar=25μm.
- (E) Representative Immunofluorescence images of the crypt for proliferating (MKI67) epithelial cells (CDH1) and the quantification of MKI67-positive epithelial cells and the length of epithelium (epithelial length/total tissue thickness). Samples from two derivations/experiments. HIO/ENS (C1/C2): n = 4. HIO/ENS/Mac (C1/C2/C3 and C1/C2/C5): n = 6. p=0.0264. p=0.3961. Welch's t-test. Student's t-test. Mean & s.d. Scale bar=25μm.
- (F) Isometric force measurements of grafted organoids with or without combined macrophages. Each row represents an individual grafted organoid sample. Quantification of maximal force recorded, ratio of time required for relaxation to contraction, and frequency of contraction. See STAR Methods. HIO/ENS/Mac (C1/C2/C3), n = 6, HIO/ENS (C1/C2), n = 3. p = 0.7303, p = 3252, p = 0.2904, Welch's t-test. Mean & s.d.



C GSEA: Top 20 enriched in IntMac(d127vs.d80)



GSEA: Top 20 enriched in OrgMac(d121vs.d37)



D d47 ◀ Mac: Int ▶ d127 d59 ◀ Mac: Int ▶ d101 d85 ◀ Mac: Int ▶ d132

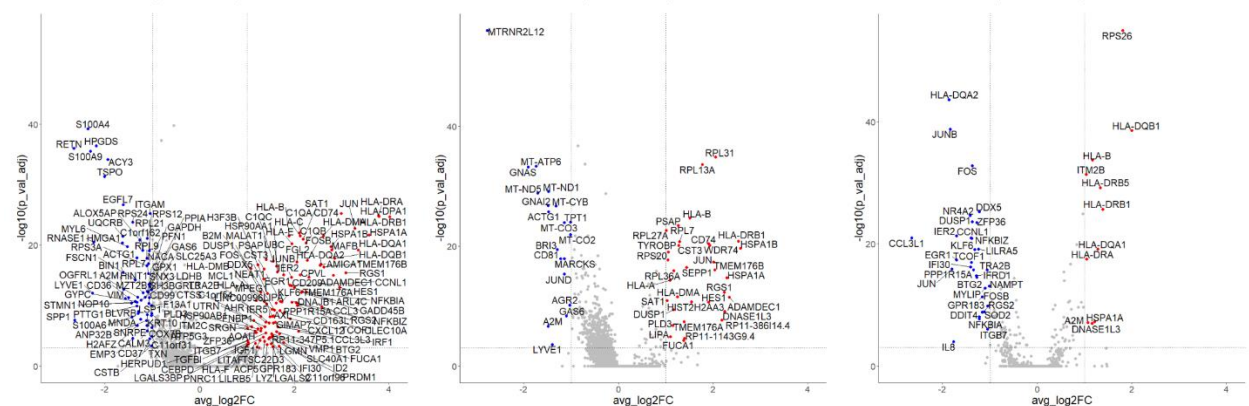


Figure S4. scRNAseq analyses of fetal intestine and organoid macrophages, related to Figure 4.

- (A) Heatmap of all 77 upregulated genes in fetal intestinal macrophages between day 127 and day 80.
- (B) Gene ontology annotations of differentially expressed genes from for commonly upregulated genes between fetal intestinal and organoid macrophages and upregulated only in fetal intestinal macrophages.
- (C) Gene Set Enrichment Analysis (GSEA). Top 20 biological process (by NES) enriched in each fetal intestinal or organoid macrophages. FDR q-value cut off < 0.25 .
- (D) Volcano plots of differentially expressed genes in fetal intestinal macrophages between day 127 vs. day 47, day 101 vs. day 59, day 132 vs. day 85. Threshold of discovery (dotted line), \log_2 fold change > 1 , adjusted p-value < 0.001 , Wilcoxon rank sum test.

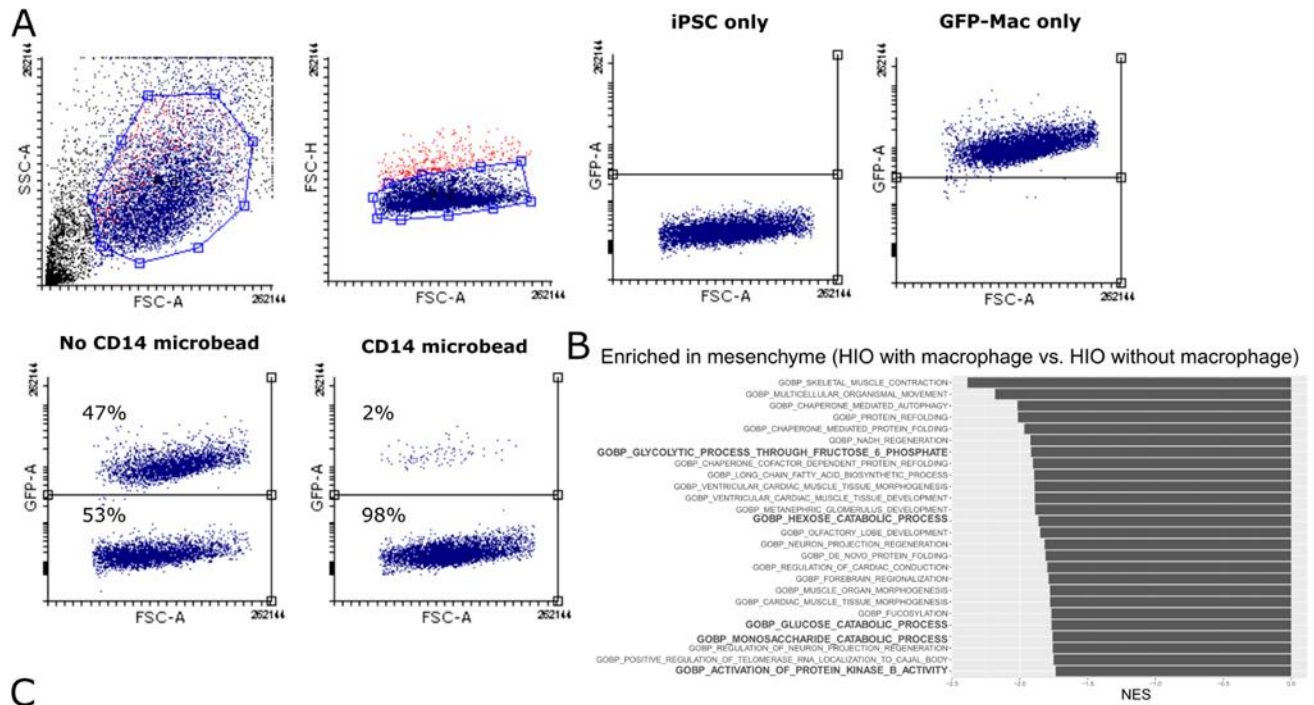


Figure S5. Efficiency of macrophage removal using magnetic microbead, related to Figure STAR Methods & Figure 6.

- (A) Efficiency of macrophage removal with microbead. Left, gating for cytometry of 1:1 cell mix of hiPSC^{WT} and hiPSC^{eGFP}-derived macrophage. Right, percent GFP-positive cells with only hiPSC^{WT} or only hiPSC^{eGFP}-derived macrophage. Bottom, percent GFP-positive macrophages of the cell mix either without or with anti-CD14 microbead mediated macrophage removal.
- (B) Gene Set Enrichment Analysis (GSEA). All 26 significant biological processes enriched from comparing mesenchymal cells from HIO or HIO/Mac. FDR q-value cut off < 0.25.
- (C) Enrichment plots of associated with glucose metabolism from (B).

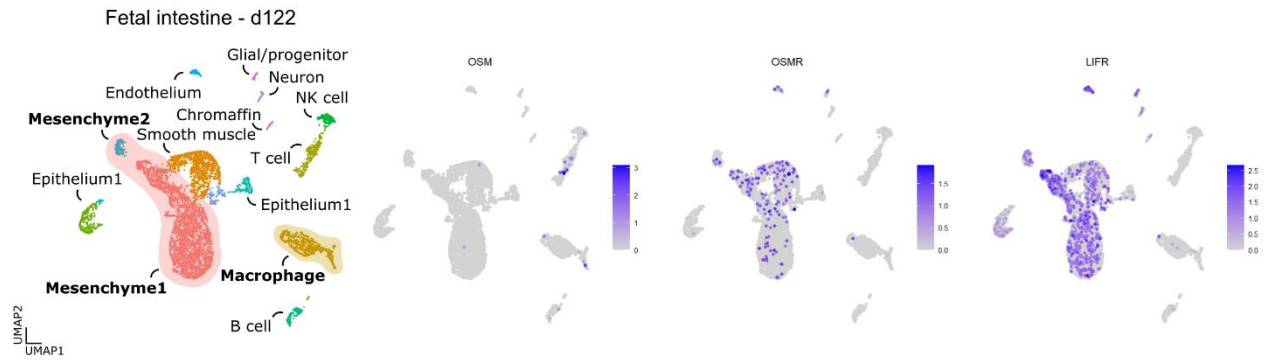
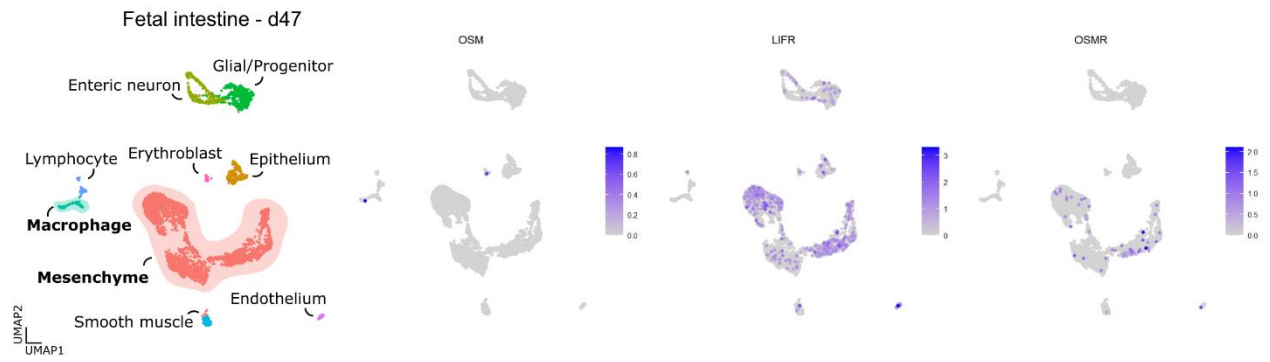


Figure S6. Expression of OSM, LIFR, and OSMR in the fetal intestines, related to Figure 7.

UMAP plot of day 47 and day 122 fetal intestine scRNAseq datasets and corresponding plots showing gene expression of OSM, LIFR, and OSMR.

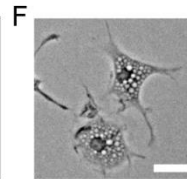
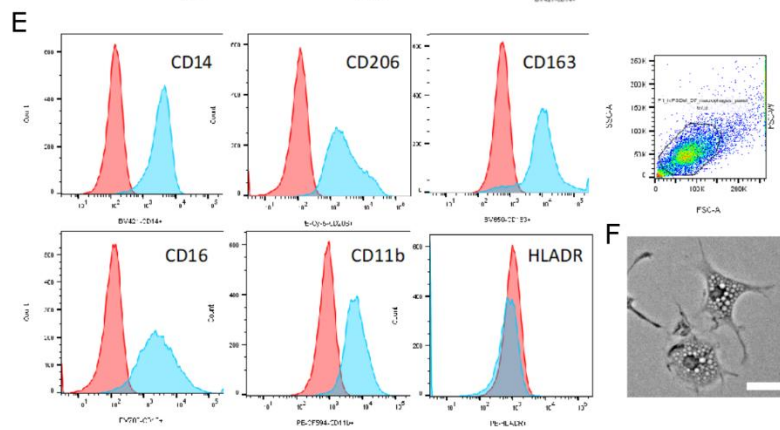
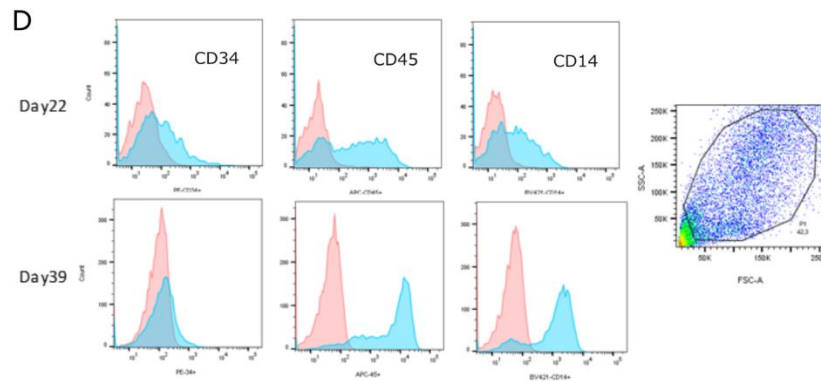
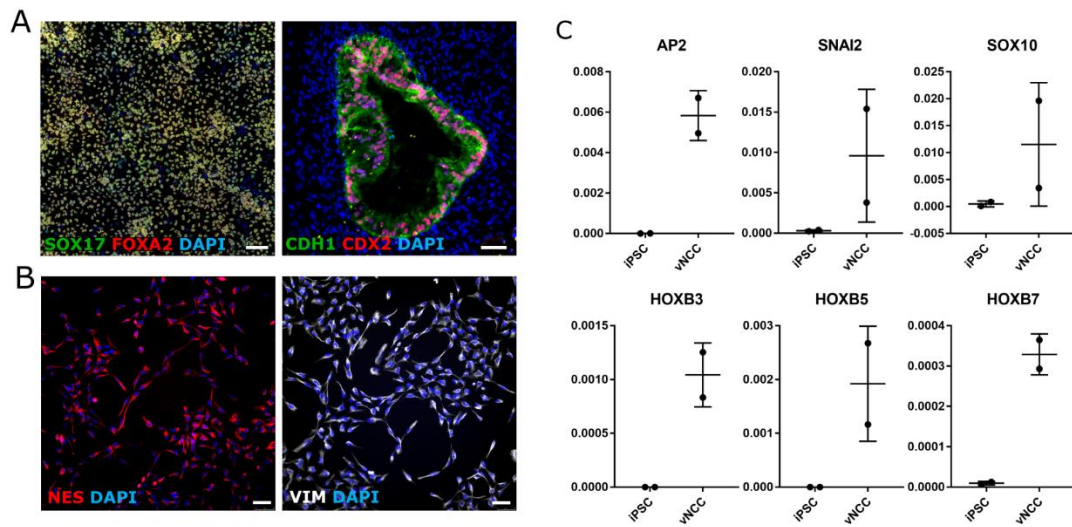


Figure S7. Characterization of hiPSC-derived human intestinal organoid, vagal neural crest, and macrophage, related to STAR Methods.

(A) Immunocytochemistry of markers for definitive endoderm (SOX17, FOXA2) and nucleus (DAPI) of endoderm monolayer during HIO derivation. Immunofluorescence of intestinal epithelial markers (CDH1, CDX2) in day 28 HIO. Scale bar=50µm.

(B) Immunocytochemistry for neural crest cell marker (NES, VIM) on the vagal neural crest cells. Scale bar=50µm.

(C) qPCR for genetic markers of neural crest (AP2, SNAI2, SOX10) and vagal fate (HOXB3, HOXB5, HOXB7) on the vagal neural crest cells (C1, C2). Normalized to GAPDH expression. hiPSC, n = 2, VNCC, n = 2. Biological replicates. Mean & s.d.

(D) Flow cytometry histograms showing staining (shaded blues) compared to the compensated unstained control (shaded red) for cell surface markers CD34, CD45 and CD14 on pre-macrophages released from adherent factory embryoid bodies (f-EB) harvested at day 22 and 39 since the beginning of the differentiation and the gating.

(E) Flow cytometry histograms showing cell surface markers CD14, CD206, CD163, CD16, CD11b and HLADR on macrophages differentiated from pre-macrophages and the gating.

(F) Bright field image of the differentiated macrophages. Scale bar=25µm.

Table S1. Oligonucleotides, related to Figure 2, 7, and S6.

Species	Target gene	Direction	Primer sequence
Human	<i>CCR2</i>	Forward	GGCATAGGGCAGTGAGAGTC
Human	<i>CCR2</i>	Reverse	TGTGAAAAAGGCTTCTGAACTTCT
Human	<i>CCR1</i>	Forward	TCCCTTGGAACCAGAGAGAAG
Human	<i>CCR1</i>	Reverse	ACCAAGGAGTACAGAGGGGG
Human	<i>CCR4</i>	Forward	AAAGCAAGCTGCTTCTGGTTG
Human	<i>CCR4</i>	Reverse	CTCCCCAAATGCCTTGATGC
Human	<i>CCR5</i>	Forward	ATCCAGTGAGAAAAGCCCGT
Human	<i>CCR5</i>	Reverse	TTCCACCCGGGGAGAGTTT
Human	<i>CCR6</i>	Forward	AAGAGAGGGCCCACGTGTAT
Human	<i>CCR6</i>	Reverse	ATTGATTCCCCGCTCATTGTG
Human	<i>CX3CR1</i>	Forward	TGGCCAAACACTGAGACCAA
Human	<i>CX3CR1</i>	Reverse	TGAAGGCCTCTAGTCGCTGT
Human	<i>CSF1R</i>	Forward	GTGGCTGTGAAGATGCTGAA
Human	<i>CSF1R</i>	Reverse	CCTTCCTTCGCAGAAAGTTG
Human	<i>FLT3</i>	Forward	CTCCAGGCGGCATCGC
Human	<i>FLT3</i>	Reverse	AAAACAACGAGCAGCGGCA
Human	<i>AP2</i>	Forward	ATGCTTTGGAAATTGACGGA
Human	<i>AP2</i>	Reverse	ATTGACCTACAGTGCCCAGC
Human	<i>SOX10</i>	Forward	AGCTCAGCAAGACGCTGG
Human	<i>SOX10</i>	Reverse	CTTTCTTGCTGCATACGG
Human	<i>SNAI2</i>	Forward	TGACCTGTCTGCAAATGCTC
Human	<i>SNAI2</i>	Reverse	CAGACCCTGGTTGCTTCAA
Human	<i>HOXB3</i>	Forward	CGTCATGAATGGGATCTGC
Human	<i>HOXB3</i>	Reverse	ATATTCACATCGAGCCCCAG
Human	<i>HOXB5</i>	Forward	GGAAGCTTCACATCAGCCAT
Human	<i>HOXB5</i>	Reverse	GGAACTCCTTTTCCAGCTCC
Human	<i>HOXB7</i>	Forward	AACTTCCGGATCTACCCCTG
Human	<i>HOXB7</i>	Reverse	CTTTCTCCAGCTCCAGGGTC
Human	<i>GAPDH</i>	Forward	GAAGGTGAAGGTCGGAGT
Human	<i>GAPDH</i>	Reverse	GAAGATGGTGATGGGATTTT
Human	<i>ENO1</i>	Forward	TCTCTTCACCTCAAAAGGTCTCT
Human	<i>ENO1</i>	Reverse	TGTGGGTTCTAAGGCTTACCC
Human	<i>TPI1</i>	Forward	GGACTCGGAGTAATCGCCTG
Human	<i>TPI1</i>	Reverse	GTACTTCCTGGGCCTGTTGG
Human	<i>LDHA</i>	Forward	CTGGCAAAGTGGATATCTTGAC
Human	<i>LDHA</i>	Reverse	ACTCCATACAGGCACACTGG
Human	<i>PGK1</i>	Forward	TTGACCGAATCACCGACCTC
Human	<i>PGK1</i>	Reverse	AGCAGCCTTAATCCTCTGGTT
Human	<i>PFKP</i>	Forward	AGGCAGTCATCGCCTTGCTAGA
Human	<i>PFKP</i>	Reverse	ATCGCCTTCTGCACATCCTGAG
Human	<i>HPRT1</i>	Forward	CCTGGCGTCGTGATTAGTGA
Human	<i>HPRT1</i>	Reverse	CGAGCAAGACGTTTCAGTCCT